

pubs.acs.org/jced Article

Exploring the Physicochemical Properties and PC-SAFT Modeling of a Mixture of Deep Eutectic Solvent (Choline Chloride and Butyric Acid) + Water

Aafia Sheikh,* Ariel Hernández,* and Athar Yaseen Khan



Cite This: https://doi.org/10.1021/acs.jced.5c00423



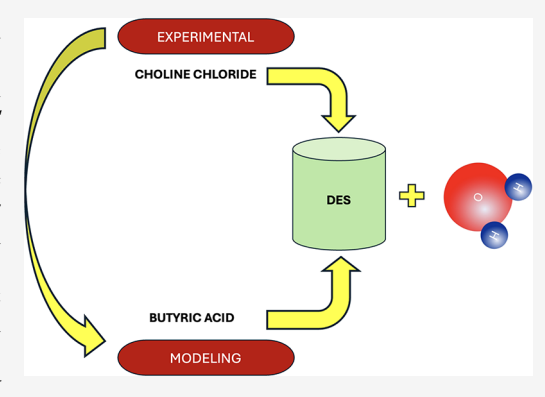
ACCESS I

Metrics & More

Article Recommendations

Supporting Information

ABSTRACT: This study reports measurement of density (ρ) , speed of sound (u), and dynamic viscosity (η) of a choline chloride and butyric acid deep eutectic solvent (ChCl/BA DES) and investigates its physicochemical properties and its aqueous mixtures for the entire range of composition at T=303.15-343.15 K. The density data are fitted by the second-degree polynomial equation in T, and the fourth-degree polynomial equation in the mole fraction of ChCl/BA DES (x_1) is fitted well for both ρ and η . Excess molar volume (V^E) shows a positive deviation from ideality with the minimum centered at $x_1\approx 0.5$. Viscosity deviation $(\Delta\eta)$ exhibits a minimum at $x_1\approx 0.5$, aligning with V^E behavior and confirming mixture stability. Isentropic compressibility deviation $(\Delta\kappa_S)$ shows a negative deviation with a minimum at $x_1\approx 0.15$. Excess properties $(V^E, \Delta\kappa_S \text{ and } \Delta\eta)$ are correlated by the Redlich–Kister (R-K) polynomial equation. The molar volume (V), lattice energy



 $(U_{\rm pot})$, molar entropy (S^0) , and intermolecular free length $(L_{\rm f})$ are evaluated to understand the derived thermodynamic properties. Temperature dependence of η is compared using Vogel–Fulcher–Tammann (VFT) and Arrhenius equations. The PC-SAFT equation of state quantitatively predicts ρ and $V^{\rm E}$ of a pseudo-binary mixture composed of a DES and water with improved accuracy using the fitted approach.

1. INTRODUCTION

Following green chemistry principles, the goal is to develop processes that eliminate the use of hazardous raw materials, minimize waste and byproduct generation, and reduce the energy consumption for material production. These processes for the development of materials are designed without compromising their physicochemical properties. Deep eutectic solvents (DESs) were first described as mixtures of quaternary ammonium chlorides with a variety of carboxylic acids. Substantial depression in the freezing point and lattice energy of the resulting mixture is attributed to strong hydrogen bonding between the chloride anion and the carboxylate group. DESs are binary or ternary mixtures of Lewis/Bronsted acids and bases at a certain mole ratio that are able to associate through hydrogen bonding. 3,4

Ionic liquids (ILs), predecessors of DESs, are known as nonvolatile, nonflammable, and water-stable solvents. ILs are reflected as species being solely composed of ionic species due to the availability of a large combination of cations and anions. With expansion in chemical diversity, structural classification, synthesis routes, and application of ILs, many of them are found to be less sustainable. DESs have emerged as an alternative class of environmentally friendly solvents to address the limitations associated with ILs. The terms DES and ILs are often used interchangeably due to many shared physicochem-

ical properties.⁶ The making of a DES is relatively inexpensive and straightforward, posing no laborious purification steps and disposal problems. DESs have gained recognition as sustainable and renewable solvents largely due to their tunable nature, which allows for the optimization of key physicochemical properties such as selectivity, viscosity, and solubility in molecular solvents for specific applications. DESs have shown utility in a wide range of industrial applications, including power systems, battery technology, gas separation, biocatalysis, gas capture, biomass processing, electrodeposition, metallurgy, organic synthesis, pharmaceuticals, medical research, and nanomaterial synthesis and functionalization. 9-14 The frequently prepared type III DESs are more sustainable and biodegradable due to the nature, composition, and concentration of components. They are prepared from readily available precursors of biological significance or those derived from natural resources such as organic acids, choline derivatives, amino acids, vitamins, sugars, and polyols. 15,16

Received: June 20, 2025 Revised: August 24, 2025 Accepted: August 26, 2025



DESs are classified as "moderately toxic" compared to their corresponding ILs.¹⁷ A comprehensive understanding of the action mechanism, physicochemical properties, and their influencing factors is essential for their effective use in targeted applications. The possible combinations of hydrogen bond donors (HBDs) and hydrogen bond acceptors (HBAs) to make DESs are infinite. For the prediction and optimization of their properties, theoretical models have been employed. However, the nature and types of interactions between HBAs and HBDs require their meaningful evaluation at the molecular level. 18,19 The presence of water can significantly impact the chemical reactivity and solvation properties of DESs by transforming the hydrogen bonding network. Therefore, understanding the effect of water on stability of DESs is essential for optimizing their physical properties for practical applications.²⁰

Choline-based DESs are biocompatible and degrade completely under aerobic conditions. They have great potential for processing lignocellulose biomass. Butyric acid (BA) is a short-chain fatty acid that finds its applications in the chemical industry, pharmaceuticals, food technology, and as animal feed. It is prepared from a petroleum derivative, propylene, by a chemical route. The biobased butyric acid can be produced from renewable sources such as agro-industry and forestry sector. Sample of the produced from renewable sources such as agro-industry and forestry sector.

There is no established approach that solely relies on HBA and HBD chemistry for tailoring and tuning of physicochemical properties of DESs.²⁴ The relatively higher viscosity of DESs often imposed a restriction on their practical applications. The stability, dissolution ability, and evaluation of thermodynamic properties of DESs in a variety of molecular solvents such as water, dimethyl sulfoxide (DMSO), and alcohols of different chain lengths expand their applications in various engineering applications...^{25–27} Water is the most abundant, environmentally friendly cosolvent in modifying the physicochemical properties of DESs that helps to understand different types of interactions (ion-ion, ion-solvent, and solvent-solvent) and structural changes in binary mixtures. 28,29 The dielectric constant, relative polarity, and hydrogen bonding network of water facilitate the dissolution of active pharmaceutical ingredients (APIs) in DES/water binary mixtures.^{30–32}

This study comprehensively investigates the physical (density, speed of sound, and dynamic viscosity) properties of choline chloride (ChCl)/BA DES and its binary mixtures with water for the entire range of composition at T=303.15-343.15 K. To understand the intermolecular interactions, the volumetric properties (excess molar volume, apparent molar volume, and partial molar volume), acoustic parameters (isentropic compressibility, isentropic compressibility deviation, intermolecular free length, and acoustic impedance), and viscosity properties (viscosity deviation) are also calculated. The Vogel–Fulcher–Tamman (VFT) and Arrhenius equations are employed to fit the experimental viscosity data. The functional dependence of volumetric and viscosity properties on the temperature and composition is discussed.

Finally, we treat DES as a pseudopure fluid and the DES + water mixture as a binary system. The perturbed chain statistical associating fluid theory (PC-SAFT) equation of state (EoS)^{33,34} was employed as a predictive approach and fitted approach for modeling the experimental density and excess molar volume for the mixture.

1.1. PC-SAFT Equation of State. In our previous work³⁵ related to the study of DES + 1-butanol, the PC-SAFT EoS was successfully applied for the fit of density in the binary mixture. In this work, we will use PC-SAFT for modeling the experimental data of density and excess molar volume. According to PC-SAFT, the liquid density can be obtained from eq 1:

$$P = \tilde{\rho} \left(\frac{\partial a}{\partial \tilde{\rho}} \right)_{T,V} - a \tag{1}$$

where $\tilde{\rho}$ represents the molar density, a denotes the Helmholtz energy density, T indicates the temperature, and V represents the molar volume. The expression for the Helmholtz energy density can be obtained from the scientific literature. ^{33,34} On the other hand, the excess molar volume, $V^{\rm E}$, is given by eq 2:

$$V^{E} = \frac{1}{\tilde{\rho}} - \frac{x_{1}}{\tilde{\rho}_{1}} - \frac{(1 - x_{1})}{\tilde{\rho}_{2}}$$
 (2)

where the subscripts 1 and 2 are related to pure fluid 1 and 2, respectively, and x denotes the mole fraction in the liquid phase.

Each pure fluid needs five adjustable parameters: the energy parameter (ε) , the temperature-independent segment diameter (σ) , the segment number (m), the effective volume (κ^{AB}) , and the association energy parameter (ε^{AB}) . After the parameters for pure fluids were determined, appropriate mixing rules must be used for binary mixtures. The cross-dispersive energy parameter includes the binary interaction parameter, k_{ij} , which accounts for attractive dispersion forces between i and j molecules. Typically, k_{ij} is fitted using phase equilibrium data or experimental data of density or excess molar volume to improve the accuracy of these properties. In this study, we will use two approaches that are related to the value of the binary interaction parameter, i.e., a predictive approach with $k_{ij} = 0$, and a fitted approach, where k_{ij} is fitted to the experimental data of excess molar volume.

2. EXPERIMENTAL METHODS

2.1. Materials. The details of chemicals used in this work are listed in Table 1 with their CAS number, source, and purity.

Table 1. CAS Registry Number, Source, and Purity of Chemicals

chemical	CAS reg. no.	source	purity wt fraction ^a	purification method			
choline chloride	67-48-1	Sigma-Aldrich	≥99	used as received			
butyric acid	107-92-6	Sigma-Aldrich	≥99	used as received			
deionized water		Sigma-Aldrich					
^a Provided by the supplier.							

2.2. Methods. 2.2.1. Preparation of the Deep Eutectic Solvent (ChCl/BA DES). The ChCl/BA DES was prepared following the procedure already reported. ^{36–38}

Choline chloride (HBA) and butyric acid (HBD) were mixed in a 1:2 molar ratio. The mixture was heated in a round-bottom flask at 343.15—348.15 K with constant stirring. The round-bottomed flask was fitted with a condenser, with a

Table 2. Density, $\rho/\text{kg·m}^{-3}$, of ChCl/BA DES and ChCl/BA DES—Water Mixtures in the Temperature Range $T=303.15-343.15~K~(x_1=\text{Mole Fraction of ChCl/BA DES})$ and Pressure $P=0.1~\text{MPa}^a$

					$ ho/{ m kg\cdot m^{-3}}$				
x_1	303.15 K	308.15 K	313.15 K	318.15 K	323.15 K	328.15 K	333.15 K	338.15 K	343.15 K
0.00	995.700	994.087	992.271	990.271	988.096	985.758	983.265	980.624	978.115
0.10	1009.88	1006.63	1003.24	999.889	996.515	993.120	989.748	986.357	982.978
0.20	1012.93	1009.61	1006.25	1002.9	999.501	996.127	992.752	989.362	985.954
0.30	1015.82	1012.52	1009.27	1005.74	1002.41	999.034	995.651	992.252	988.868
0.40	1018.71	1015.33	1011.95	1008.56	1005.24	1001.86	998.457	995.055	991.664
0.50	1022.73	1019.35	1015.86	1012.64	1009.19	1005.79	1002.39	999.032	995.584
0.60	1027.48	1024.11	1020.73	1017.37	1013.99	1010.64	1007.34	1003.84	1000.50
0.70	1031.21	1027.82	1024.45	1021.06	1017.67	1014.36	1010.91	1007.56	1004.19
0.80	1034.50	1031.12	1027.84	1024.41	1021.08	1017.71	1014.46	1011.04	1007.75
0.90	1037.16	1033.77	1030.41	1027.15	1023.73	1020.42	1017.07	1013.74	1010.39
1.00	1039.72	1036.36	1033.00	1029.65	1026.30	1022.98	1019.66	1016.34	1013.04

[&]quot;Standard uncertainties u in T, x_1 , P, and ρ are u(T) = 0.01 K, $u(x_1) = 0.01$, u(P) = 10 kPa, and $u_r(\rho) = 0.001$ kg·m⁻³, respectively.

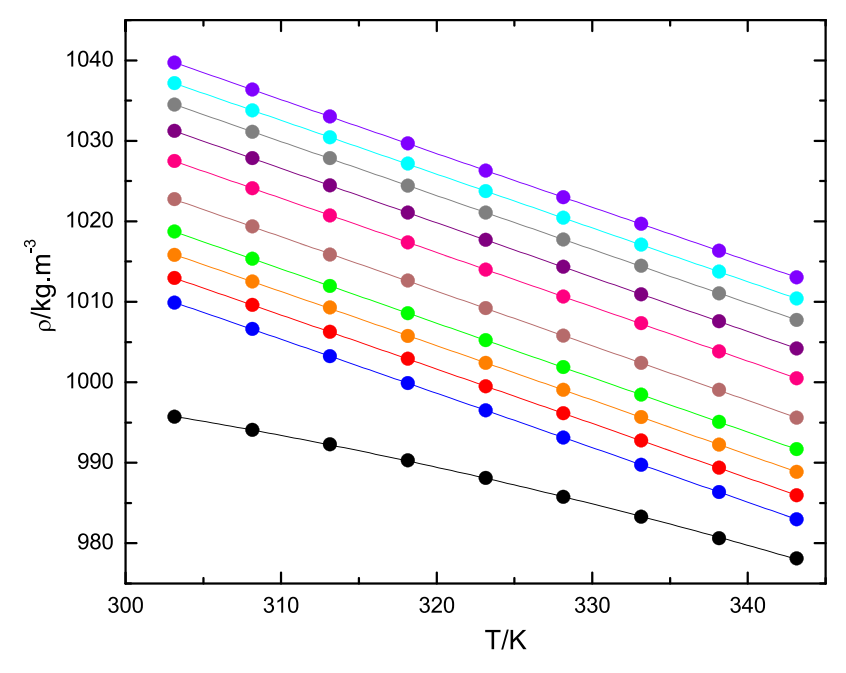


Figure 1. Temperature, T, dependence of density, ρ , of ChCl/BA DES—water mixtures for different mole fractions of ChCl/BA DES ($x_1 = 0.0$; solid blue circle: 0.1; solid red circle: 0.2; solid orange circle: 0.3; solid green circle: 0.4; solid brown circle: 0.5; solid pink circle: 0.6; solid purple circle: 0.7; solid gray circle: 0.8; solid skyblue circle: 0.9; solid violet circle: 1.00). The solid lines are the best fit representation of eq 3.

drying tube filled with silica gel attached at its end. The contents of the flask were continuously stirred until a homogeneous, colorless, and transparent liquid of the ChCl/BA DES formed. The prepared DES was allowed to cool to room temperature, stored in a sealed bottle, and kept in a desiccator to avoid moisture absorption and contamination. The moisture content of the prepared ChCl/BA DES was determined with the coulometric Karl Fischer titration equipment (Mettler Toledo, V10S) using Karl Fischer reagent (CombiNorm5 and methanol) which was 0.04 wt %. Considering the possible sources of errors in the weighing process, the estimated relative uncertainty of ChCl and butyric acid ratio r was $U_r(r) \approx 0.0003$.

2.2.2. Characterization. The prepared ChCl/BA DES was characterized by Fourier transform infrared (FTIR) and NMR spectroscopy.

2.2.2.1. FTIR Spectral Analysis. FTIR spectra of choline chloride (ChCl), ChCl/BA DES, and butyric acid (BA) were recorded on an FTIR spectrometer (Alpha Bruker II). The

recorded FTIR spectra of ChCl, ChCl/BA DES, and BA are shown in Figure S1 (Supporting Information).

The FTIR spectra of ChCl/BA DES and water binary mixtures corresponding to mole fractions ($x_1 = 0.0, 0.1, 0.3, 0.5, 0.7, 0.9, 1.0$) were also recorded and are shown in Figure S2.

2.2.2.2. NMR (¹H and ¹³C) Spectral Analysis. The NMR (¹H and ¹³C) spectra of the prepared ChCl/BA DES were recorded on a Bruker Avance 300 MHz spectrometer. These spectra are shown in Figures S3 and S4 (Supporting Information).

2.2.3. Preparation of a Binary Mixture of ChCl/BA DES and Water. Binary solutions of ChCl/BA DES and deionized water over the entire range of composition ($x_1 = 0.0-1.0$) were prepared by weighing components in airtight glass vials using an analytical balance (Shimadzu AUW220D). The aqueous binary mixtures of ChCl/BA DES were stirred to ensure homogeneous solutions.

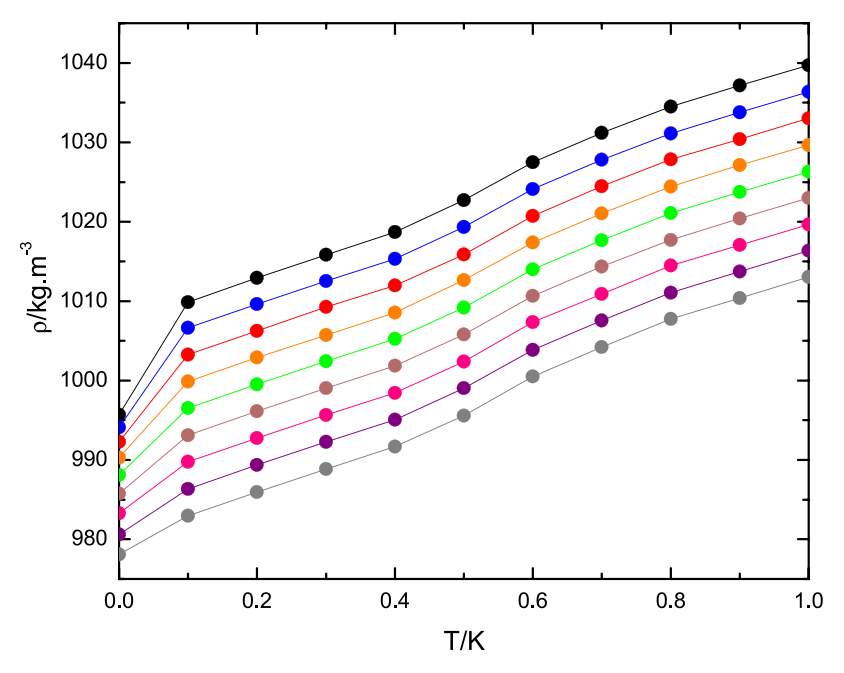


Figure 2. Variation of density ρ of ChCl/BA DES—water mixtures with the mole fraction of ChCl/BA DES, x_1 , in the temperature range 303.15 \leq $T/K \leq$ 343.15 (\bullet : 303.15 K; solid blue circle: 308.15 K; solid red circle: 313.15 K; solid orange circle: 318.15 K; solid green circle: 323.15 K; solid brown circle: 328.15 K; solid pink circle: 333.15 K; solid purple circle: 338.15 K; solid gray circle: 343.15 K). The solid lines are the best fit representations of eq 4.

2.2.4. Measurement of Density and Speed of Sound. The density and speed of sound metering instrument (DSA 5000 M, Anton Paar) was used for density (ρ) and speed of sound (u) measurements of ChCl/BA DES and its binary mixtures with water in the 303.15-343.15 K temperature range at 5 K intervals. The two-in-one instrument is equipped with a density and speed of sound measuring cell combined with the oscillating U-tube method. Both cells were temperature controlled by a built-in Peltier thermostat with an uncertainty of 0.01 K. The density was measured by a vibrating tube densimeter. Density was derived from the resonant frequency of the sample-filled U-shaped tube as it vibrated perpendicular to its plane within an electromagnetic field. The vibration was considered as a simple harmonic oscillation. The ultrasonic transducer frequency of the DSA 5000 M was 3 MHz. The speed of the sound was derived by determining the period of received sound waves and by considering the distance between the transmitter and receiver. Prior to each measurement, the instrument was calibrated with deionized water and air according to the instructions given in the user manual provided by Anton Paar. The measuring tube of DSA 5000 M was thoroughly cleaned several times with deionized water, rinsed with ethanol, and dried by using a blower before injecting each sample.

2.2.5. Measurement of Dynamic Viscosity. A viscosity module (Lovis 2000 M/ME, Anton Paar) coupled to DSA 5000 M was used for viscosity measurements of ChCl/BA DES and its aqueous binary mixtures in the temperature range 303.15-343.15 K. The dynamic viscosity (η) measurements are based on the falling ball principle. The temperature uncertainty and repeatability factor of DSA 5000 M and Lovis Module 2000 M/ME were 0.01 0.02, 0.01, and 0.005 K, respectively, according to their user manuals provided. Viscosity measurements were made with capillary tubes of diameter 1.59, 1.8, and 2.5 mm, respectively, which were calibrated at different temperatures and angles of inclination,

with viscosity standards (S3, S6, N100, and N415) supplied by Anton Paar.

The working equations of DSA 5000 M and Lovis module 2000 M/ME are given in the Supporting Information, eqs S1 and S2.

3. RESULTS AND DISCUSSION

3.1. Density. The measured experimental density ($\rho/\text{kg} \cdot \text{m}^{-3}$) data of ChCl/BA DES and its aqueous mixtures for the entire range of composition at T = 303.15 - 343.15 K are given in Table 2. The temperature dependence of ρ is modeled with eq 3, and the corresponding ρ vs T plots are shown in Figure 1.

$$\rho = \sum_{j=0}^{2} a_j T^j \tag{3}$$

The three fitting parameters a_j of eq 3 and r^2 (goodness of fit) values are given in Table S2 (Supporting Information).

Figure 1 demonstrates that density (ρ) increases with an increase in the mole fraction (x_1) of ChCl/BA DES, while it decreases with an increase in T. The decrease in density can be attributed to thermal expansion of the liquid volume with temperature increase, resulting in less dense mixtures at higher temperatures. The change in ρ with respect to T is linear for pure DES and their higher mole fractions with water; however, this linearity changes by decreasing the amount of DES or increasing the amount of water in the ChCl/BA DES binary mixture. The formation of a bond increases with increasing concentration of DES resulting in higher density for neat DES compared to their aqueous mixtures. Statistically, the goodness of fit is represented by r^2 , also reported by other authors. $^{40-42}$

The ρ of ChCl/BA DES increases with x_1 at constant T. However, for ChCl/BA DES aqueous binary mixtures (with increasing water content), a decrease in ρ with x_1 T is observed with increasing T (Figure 2). The measured density data are

Table 3. Excess Molar Volume, $V^{\rm E} \times 10^7 / {\rm m}^3 \cdot {\rm mol}^{-1}$, of ChCl/BA DES-Water Mixtures at Different Temperatures^a

	$V^{\rm E} \times 10^7/{ m m}^3 \cdot { m mol}^{-1}$								
x_1	303.15 K	308.15 K	313.15 K	318.15 K	323.15 K	328.15 K	333.15 K	338.15 K	343.15 K
0.00	0	0	0	0	0	0	0	0	0
0.10	0.701	0.964	1.232	1.464	1.676	1.870	2.034	2.182	2.352
0.20	2.886	3.145	3.392	3.613	3.829	4.017	4.186	4.341	4.528
0.30	4.628	4.854	5.037	5.322	5.502	5.687	5.861	6.024	6.205
0.40	5.889	6.127	6.348	6.560	6.719	6.900	7.083	7.250	7.434
0.50	6.008	6.215	6.477	6.565	6.779	6.958	7.131	7.265	7.478
0.60	4.990	5.152	5.315	5.456	5.600	5.725	5.812	6.027	6.152
0.70	3.974	4.113	4.235	4.367	4.493	4.563	4.742	4.835	4.964
0.80	2.727	2.819	2.832	2.966	3.014	3.106	3.100	3.232	3.271
0.90	1.526	1.589	1.632	1.585	1.683	1.696	1.753	1.787	1.858
1.00	0	0	0	0	0	0	0	0	0

"Standard uncertainties, u, in T, x_1 , P, and ρ are u(T) = 0.01 K, $u(x_1) = 0.01$, u(P) = 10 kPa, and $u_r(\rho) = 0.001$ kg·m⁻³, respectively, and $u(V^E) = 0.06 \times 10^{-7}$ m³·mol⁻¹.

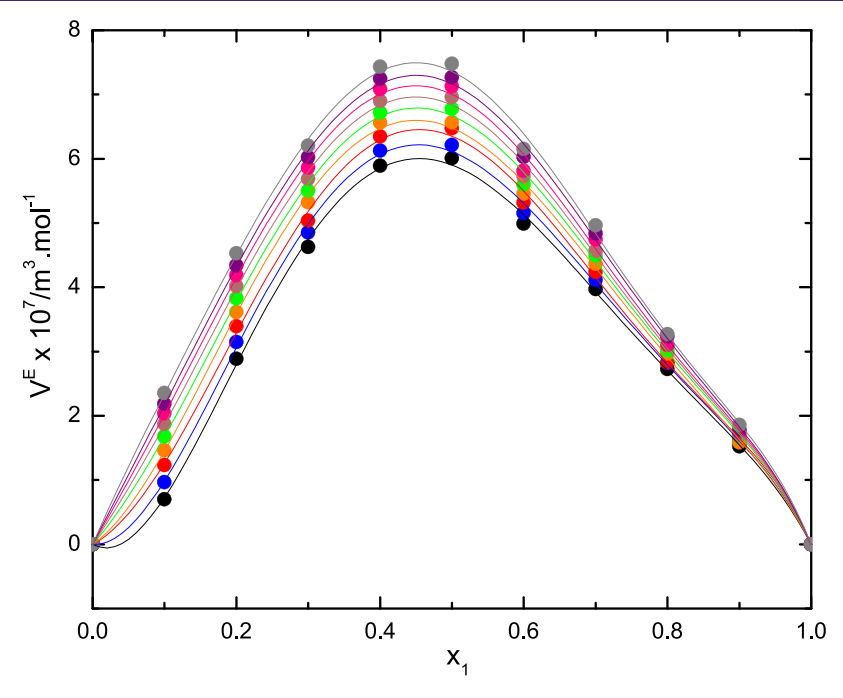


Figure 3. Variation of excess molar volume, $V^{\rm E} \times 10^7 / {\rm m}^3 \cdot {\rm mol}^{-1}$, of ChCl/BA DES—water mixtures with mole fraction of ChCl/BA DES, x_1 , in the temperature range 303.15 $\leq T/{\rm K} \leq 343.15$ (\odot : 303.15 K; solid blue circle: 308.15 K; solid red circle: 313.15 K; solid orange circle: 318.15 K; solid green circle: 323.15 K; solid brown circle: 328.15 K; solid pink circle: 333.15 K; solid purple circle: 338.15 K; solid gray circle: 343.15 K). The solid lines connecting data points are the best fit representations of eq 10.

well fitted at all temperatures to a polynomial equation in x_1 , eq 4.

$$Y = \sum_{j=0}^{4} b_{j} x_{1}^{j} \tag{4}$$

where $Y = \rho$ (density) or η (dynamic viscosity), b_j is the fitting parameter according to the degree of polynomial equation, and j is the degree of polynomial equation.

The obtained correlated parameters are summarized in Table S3 (Supporting Information) together with the corresponding standard deviations of the fit σ_{fit} .

Density is influenced by the vacancies present within the DES's liquid structure. The density of pure DES and its aqueous mixtures is manipulated by the nature and structure of HBA and HBD, their molar ratio, and the composition changes in addition to temperature and pressure. The availability of free

spaces at higher T increases due to the reduction of number of hydrogen bonds, resulting in faster movement of molecules with the corresponding decrease in density of ChCl/BA DES.

The variation in ρ of DES can be correlated using an isobaric thermal expansion coefficient $\alpha_{\rm P}$, which is a measure of contraction or expansion behavior of DES as a function of temperature.

 $\alpha_{\rm P}$ is calculated using eq 5.⁴³ The resulting values are collected in Table S4 and the corresponding $\alpha_{\rm P}$ vs x_1 plots are shown in Figure S5.

$$\alpha_{\rm p} = \frac{1}{V} \left(\frac{\partial V}{\partial T} \right)_{\rm p} = -\rho^{-1} \left(\frac{\partial \rho}{\partial T} \right)_{\rm p} \tag{5}$$

 $\alpha_{\rm P}$ determines the system's volume sensitivity to temperature increase at constant pressure. The magnitude of $\alpha_{\rm P}$ decreases with increasing temperature for all compositions. It measures

the ease with which the liquid expands with temperature at constant pressure. Since α_P depends upon the HBA/HBD mole ratio and ionic capacity of solvent to establish electrostatic interaction between HBA and HBD, the decrease in property is attributed to strong hydrogen bonding in ChCl/BA DES's structure.⁴⁴

The molar mass of ChCl/BA DES is calculated using eq 6.45

$$M_{\text{ChCl/BA DES}} = M_{\text{ChCl}} x_{\text{ChCl}} + M_{\text{BA}} x_{\text{BA}}$$
 (6)

where M_{ChCl} x_{ChCl} and $M_{\text{BA}}x_{\text{BA}}$ are the molecular mass and mole fraction of choline chloride (ChCl) and of butyric acid (BA), respectively.

The lattice potential energy $U_{\rm pot}$ and standard molar entropy S^0 of pure ChCl/BA DES are calculated at T=303.15-343.15 K using empirical eqs 7 and 8, respectively.⁴⁶

$$U_{\text{pot}} = 1981.2(\rho/M_{\text{ChCl/BADES}})^{1/3} + 103.8$$
 (7)

$$S^0 = 1246.5V + 29.5 \tag{8}$$

where S^0 is the standard molar entropy measured in kJ·mol⁻¹ and V is the molecular volume in nm³ ($V = 10^{21} \times V_{\rm m}/N_{\rm A}$). The calculated values of S^0 , U_{pot} and V are listed in Table S5 (Supporting Information). The lattice energy U_{pot} measures the strength of ionic interactions in the system, which is affected more by the molecular mass of DES compared to its density. U_{pot} represents the energy required to remove complex ions from their structure. DESs have lower lattice energy than conventional solvents $(U_{pot}(CsI) = 613 \text{ kJ} \cdot \text{mol}^{-1})$, 47 which is the reason of its being in the liquid state at room temperature. Moreover, the liquid state of the DES precursor favors thermodynamically stable ionic solutions. With increasing T, S^0 of ChCl/BA DES increases slightly due to increased molecular mobility. S^0 values of inorganic salts, NaCl (72.1 kJ·K⁻¹·mol⁻¹) and KCl (82.6 kJ·K⁻¹·mol⁻¹) are higher than DESs and ILs.⁴⁸ This indicates more disordered structures resulting from decreased charge density and lower electrostatic energy.⁴

3.1.1. Excess Molar Volume. To account for the ideal or nonideal behavior, structural arrangements, and molecular interactions in ChCl/BA DES + water binary mixtures, the excess molar volume $V^{\rm E}$ for all binary mixtures is calculated using eq 9.

$$V^{E} = \sum_{i=1}^{2} (x_{i} M_{i}) (\rho^{-1} - \rho_{i}^{-1})$$
(9)

where x_i , M_i , and ρ_i represent the mole fraction, molar mass, and density of component i [i = 1 (ChCl/BA DES), i = 2 (water)], respectively, and ρ is the density of binary mixtures.⁵¹

The calculated V^{E} values are collected in Table 3, and plots of V^{E} vs x_{1} (x_{1} = mole fraction of ChCl/BA DES) are shown in Figure 3.

Figure 3 shows that the values of $V^{\rm E}$ are positive for the entire range of compositions and temperature investigated. For an ideal binary mixture, the $V^{\rm E}$ is nearly zero. The sign and magnitude of the excess properties ($V^{\rm E}$, $\Delta\kappa_{\rm S}$ and $\Delta\eta$) corresponds to the molecular mass of HBA and HBD, the nature of intermolecular interactions, and structural occupation in interstitial spaces which are occupied due to the existing difference in free volumes and molar volumes of components of solution. The excess property values are significantly affected by the nature and the type of physical, chemical, or structural interactions between the components of mixture. (1) The chemical and specific interactions between unlike

molecules correspond to hydrogen bonding and dipole—dipole interactions which lead to volume contraction resulting in negative contribution to V^{E} ; (2) the charge-transfer-type interaction forces and structural (geometric) fitting of components of binary mixture into each other producing more compact geometric structure, leading to negative V^{E} values. The positive V^{E} is attributed to physical contribution which are nonspecific interactions (3) steric hindrance and unfavorable accommodation of component molecules and (4) dipolar association in pure liquid or disruption in the liquid structure. The plot of V^{E} vs x_1 for all studied temperatures is found to be symmetric with the maximum lying at $x_1 = 0.5$. The V^{E} values are positive for the entire range of compositions and temperature studied, but in comparison the effect of increasing mole fraction of DES on V^{E} is more pronounced than that of temperature. The positive values of V^{E} throughout are an indicator for the overall weakening of hydrogen bonding in the mixture. 54 The positive values of V^{E} can arise from the self-association of pure components, as observed in glycerol mixtures with water and methanol. The -OH of glycerol makes a strong interaction with water compared to methanol. Similar behavior is observed in binary mixtures of 2-propanol and aromatic hydrocarbons. The steric hindrance offered by the bulky methyl groups may restrict the proper orientation of 2-propanol toward the ring structures, which leads to a stronger packing effect and electron donor-acceptor interactions became weaker.56

In water, the clustering of molecules occurs in various shapes and order, as explained by HF, DFT, and perturbation theory. The hydrogen bonding is dominant over noncovalent interactions in the liquid state. 57 The observed positive V^{E} values imply the self-association and clustering of water molecules in the ChCl/BA DES + water binary mixtures. On addition of DES in water, the intramolecular hydrogen bonding between DES and water is disrupted, and relatively weak hydrogen bonding is formed between water and the chloride ion of HBA.⁵⁸ At infinite dilution in water, the DES molecules break away from their pure environment and begin to settle in the water environment apparently in the form of ions. With increasing concentrations of ChCl/BA DES, organization among the ions takes place, depending on the degree of dissociation and subsequent hydration with water molecules. The V^{E} increases with increasing temperature at all mole fractions with the maximum centered at $x_1 = 0.5$ for all compositions. Initially, in the high-concentration water region (water-rich region), self-association and clustering are dominant. With increasing concentration of ChCl/BA DES (DES-rich region), the self-associated structures start dissociating.⁵⁹ It is also observed that the influence of nonspecific interactions on temperature change is negligible.

The molecular interaction between ChCl/BA DES and their aqueous binary mixtures can be qualitatively derived from FTIR spectral measurements at selected mole fractions. The FTIR spectra of pure DES and its aqueous binary mixtures are presented in Figure S2 (Supporting Information).

The presence of a broad peak in 3500–3000 cm⁻¹ is attributed to the stretching vibration of the –OH group. It is well known that a hydrogen-bonded –OH group produces a fairly broad peak than free –OH. The presence of hydrogen bonding is observed in neat ChCl/BA DES and higher mole fraction ($x_1 \ge 0.7$). The structure of DES remains unchanged when only 10% of water is added. However, the significant change in the shape and shifting in the spectrum of respective

Table 4. Speed of Sound, $u/\text{m·s}^{-1}$, of ChCl/BA DES-Water Mixtures as a Function of Temperature T = 303.15 - 343.15 K and Pressure P = 0.1 MPa^a

					$u/m \cdot s^{-1}$				
x_1	303.15 K	308.15 K	313.15 K	318.15 K	323.15 K	328.15 K	333.15 K	338.15 K	343.15 K
0.00	1510.1	1521.0	1530.0	1537.5	1543.5	1548.4	1551.8	1554.0	1554.7
0.10	1650.1	1645.8	1642.2	1638.5	1633.7	1629.2	1624.2	1619.9	1615.3
0.20	1670.2	1666.7	1663.2	1659.0	1654.8	1650.3	1645.3	1641.0	1636.4
0.30	1695.2	1690.6	1687.1	1683.1	1678.8	1673.9	1669.2	1665.2	1661.1
0.40	1722.5	1718.1	1714.2	1711.0	1706.3	1701.5	1696.4	1692.7	1688.4
0.50	1750.5	1745.5	1741.4	1737.1	1733.5	1728.9	1725.8	1721.4	1717.7
0.60	1773.5	1768.5	1764.4	1760.1	1757.1	1752.9	1748.8	1744.8	1741.7
0.70	1795.9	1791.7	1786.8	1782.7	1780.1	1776.1	1772.8	1769.6	1765.9
0.80	1826.2	1820.7	1816.6	1812.3	1809.3	1805.1	1802.0	1798.6	1794.9
0.90	1861.2	1855.7	1851.6	1847.3	1844.3	1840.1	1837.0	1833.6	1829.9
1.00	1901.2	1895.7	1891.6	1887.3	1884.3	1880.1	1877.0	1873.6	1869.9

^aStandard uncertainties, u, in T, x, P, and u are u(T) = 0.01 K, $u(x_1) = 0.01$, u(P) = 10 kPa, and u(u) = 0.5 m·s⁻¹, respectively.

pure components arises due to red shift of the hydroxyl band in the water-rich region $(x_1 \leq 0.3)$. The $-\text{CH}_2$ bending vibration remains nearly constant at $1468 \pm 2 \text{ cm}^{-1}$, but the intensity of the peak decreases in the water-rich region. The distinct -C=O stretching vibration is observed at $1750 \pm 2 \text{ cm}^{-1}$ for neat DES and its higher mole fractions $(x_1 \geq 0.5)$. The appearance of -C-O stretching peak at 1222 cm^{-1} in neat ChCl/BA DES and its higher mole fraction supports the presence of hydrogen bonding. Similar studies are also reported in the literature for interactions in neat DES—cosolvent systems. 60,61

The Redlich–Kister (R–K) polynomial equation is used to analyze the thermodynamic and acoustic properties of liquid mixtures and to identify and characterize the nature of molecular interactions. Algebraic sign associated with the property provides insight into the type of intermolecular interactions present in liquid mixtures. The magnitude of associative, dissociative, or other interactions reflects the extent of nonideality of the system. The R–K polynomial equation is thus an approach to analyze and explain solute—solvent interactions and discuss the nature of interactions.

The combined Redlich–Kister (R–K) model at constant T explains the relationship between excess molar properties ($V^{\rm E}$, $\Delta \kappa_{\rm S}$ and $\Delta \eta$) and composition ($\kappa_{\rm 1}$ = mole fraction of ChCl/BA DES), as given by eq 10.^{59,62–64}

$$Y^{E} = x_{\text{ChCl/BA DES}} x_{\text{water}} \sum_{j=0}^{k} A_{j} (x_{\text{ChCl/BA DES}} - x_{\text{water}})^{j}$$
(10)

where $Y^{\rm E}=(V^{\rm E}, \Delta\kappa_{\rm S} \text{ and } \Delta\eta)$, $\kappa_{\rm ChCl/BA\ DES}$ refers to the mole fraction of ChCl/BA DES (component 1), $\kappa_{\rm water}$ refers to the mole fraction of water (component 2), A_j is the adjustable binary coefficient, and j is the degree of polynomial equation.

The fitting of the excess property Y^E by the least-squares method provides meaningful insight. which helps to understand molecular interactions between components of a binary mixture. The numerical values of j can be varied to find an accurate mathematical representation of experimental data.

The calculated $V^{\rm E}$ values are satisfactorily fitted to a fourth-order R-K polynomial equation, shown as solid lines in Figure 3. The correlated adjustable polynomial coefficients $(A_j$'s) and their standard deviations (σ) are collected in Table S6 (Supporting Information).

3.1.2. Apparent Molar Volume and Partial Molar Volume. The solute—solvent and solute—solute interactions⁶⁵ in the aqueous binary mixture of ChCl/BA DES are further explained by calculating the apparent molar volume $(V_{\phi,i})$, partial molar volume $(\overline{V_i})$, and excess partial molar volume $(\overline{V_i})$ of individual components using eqs 11, 12, and 13, respectively.

$$V_{\phi,i} = V_{\mathrm{m},i} + \frac{V^{\mathrm{E}}}{x_i} \tag{11}$$

$$\overline{V_i} = V_{m,i} + V^E + (1 - x) \left(\frac{\partial V^E}{\partial x_i} \right)_{P,T}$$
(12)

$$\overline{V}_i^{E} = \overline{V}_i - V_{m,i} \tag{13}$$

where $V_{m,i}$ is the molar volume of pure component i. The calculated values of $V_{\phi,i}$, $\overline{V_i}$, and $\overline{V_i^E}$ of individual components [i = 1 (ChCl/BA DES); i = 2 (water)] are collected in Tables S7-S12 (Supporting Information). $\overline{V_i}$ is considered as the combination of volumetric contributions which include the intrinsic solute volume and the contribution due to interaction of the solute and solvent. In binary aqueous mixtures, the properties of water molecules in the hydration sphere depend on the nature of solute molecules and their interaction with water. 66 The DES-water interactions are also studied by calculating the $\overline{V}_i^{\rm E}$ of individual components. The value of $\overline{V}_i^{\rm E}$ increases with increasing T due to volume expansion (Tables S11 and S12, Supporting Information), indicating that the dissociation effect is dominant over association when DES is added in an infinite volume of water. Figure S6 shows the variation of $\overline{V}_i^{\text{E}}$ of individual components with x_1 at T = 313 K. The two curves cross each other at $x_1 = 0.5$, supporting the discussion for V^{E} .

At infinite dilution, the solute—solvent interactions can be neglected. The partial molar properties at infinite dilution provide practical information for the solute—solvent interaction independent of the concentration effect. The partial molar volumes for ChCl/BA DES (\overline{V}_1^∞) and water (\overline{V}_2^∞) are calculated using eqs 14 and 15, respectively.

$$\overline{V}_{1}^{\infty} = V_{m,1} + \sum_{i=1}^{n} A_{i} (-1)^{i}$$
(14)

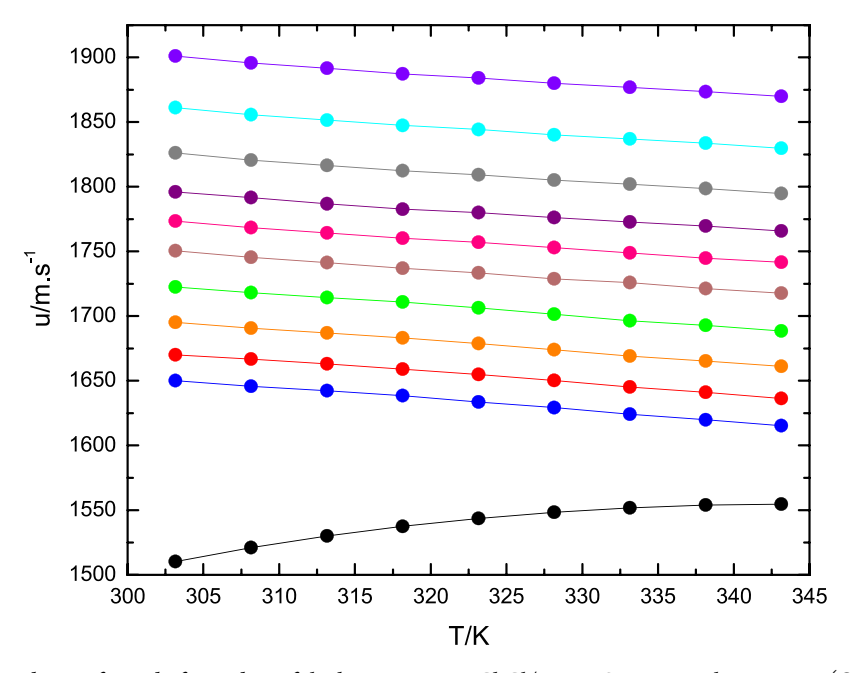


Figure 4. Temperature dependence of speed of sound, u, of the binary mixture ChCl/BA DES—water with varying x_1 (\bullet : 0.0; solid blue circle: 0.1; solid red circle: 0.2; solid orange circle: 0.3; solid green circle: 0.4; solid brown circle: 0.5; solid pink circle: 0.6; solid purple circle: 0.7; solid gray circle: 0.8; solid skyblue circle: 0.9; solid violet circle: 1.00). The solid lines connect the experimental data points.

Table 5. Isentropic Compressibility, $\kappa_S \times 10^{12}/\mathrm{Pa}^{-1}$, of ChCl/BA DES-Water Mixtures as a Function of Temperature T^a

	$\kappa_{\mathrm{S}} imes 10^{12}/\mathrm{Pa}^{-1}$								
x_1	303.15 K	308.15 K	313.15 K	318.15 K	323.15 K	328.15 K	333.15 K	338.15 K	343.15 K
0.00	440.4	434.8	430.5	427.2	424.8	423.1	422.3	422.3	423.0
0.10	363.7	366.8	369.6	372.5	376.0	379.4	383.0	386.4	389.9
0.20	353.9	356.6	359.3	362.3	365.4	368.6	372.1	375.3	378.8
0.30	342.6	345.6	348.1	351.0	354.0	357.2	360.5	363.5	366.5
0.40	330.8	333.7	336.3	338.7	341.7	344.8	348.0	350.7	353.7
0.50	319.1	322.0	324.6	327.2	329.7	332.6	335.0	337.8	340.4
0.60	309.4	312.2	314.7	317.3	319.4	322.0	324.6	327.2	329.5
0.70	300.7	303.1	305.7	308.2	310.1	312.5	314.8	316.9	319.3
0.80	289.8	292.6	294.8	297.2	299.2	301.6	303.6	305.7	308.0
0.90	278.3	280.9	283.1	285.3	287.2	289.4	291.4	293.4	295.6
1.00	266.1	268.5	270.5	272.7	274.4	276.5	278.4	280.3	282.3

^aStandard uncertainties, u, in T, x, P, and u are u(T) = 0.01 K, $u(x_1) = 0.01$, u(P) = 10 kPa, and u(u) = 0.5 m·s⁻¹, respectively.

$$\overline{V}_{2}^{\infty} = V_{\text{m},2} + \sum_{i=2}^{n} A_{i} \tag{15}$$

The calculated values of \overline{V}_1^{∞} and \overline{V}_2^{∞} are collected in Table S13 (Supporting Information).

3.2. Speed of Sound. Speed of sound (u) is a key parameter to study the intermolecular interactions within a mixture through association, dissociation, or complex formation among its components. u is closely related to several other important physical properties, including density, isentropic and isothermal compressibility, thermal conductivity, and heat capacity. Experimentally determined speed of sound of ChCl/BA DES and its binary solutions with water over the entire range of composition and at T=303.15-343.15 K is collected in Table 4, and variation of u vs u is plotted in Figure 4. The speed of sound of ChCl/BA DES and its aqueous binary mixtures decreases with increasing u7, whereas the behavior of water follows the opposite trend. The effect of mixture composition on u is more pronounced at

higher mole fractions (of water) compared with lower mole fractions.

The speed of sound of ChCl/BA DES decreases with increasing T due to decreases in the density of DES, which makes the medium less dense for traversing the sound waves. This results in slowing of the speed of sound waves.

3.2.1. Isentropic Compressibility and Isentropic Compressibility Deviation. Isentropic compressibility of ChCl/BA DES and its binary mixtures with water can be calculated in the temperature range studied using the Newton–Laplace equation⁶⁸ (eq 16).

$$\kappa_{\rm S} = -\frac{1}{V} \left(\frac{\partial V}{\partial P} \right) = \frac{1}{\rho u^2} \tag{16}$$

The calculated κ_S values from experimental data of ρ and u are reported in Table 5 as a function of temperature and composition. The compressibility parameter is indicative of available free space in liquid's structure. It represents the change in the volume of fluid with the corresponding change in

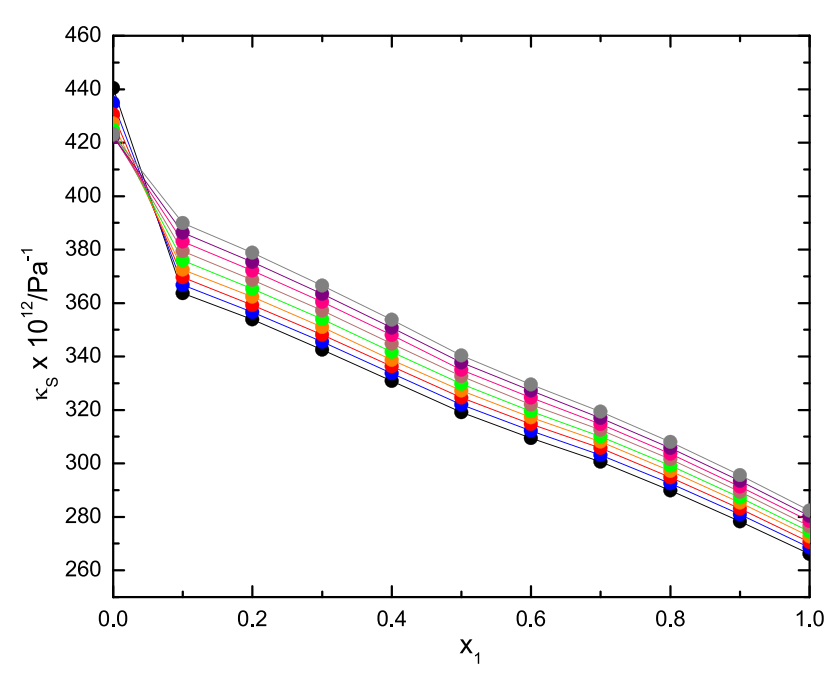


Figure 5. Isentropic compressibility, $κ_S × 10^{12}/Pa^{-1}$, of ChCl/BA DES—water mixtures as a function of $κ_1$ in the temperature range 303.15 ≤ T/K ≤ 343.15 (●: 303.15 K; solid blue circle: 308.15 K; solid red circle: 313.15 K; solid orange circle: 318.15 K; solid green circle: 323.15 K; solid brown circle: 328.15 K; solid pink circle: 333.15 K; solid purple circle: 338.15 K; solid gray circle: 343.15 K). The solid lines connect data points calculated from eq 17.

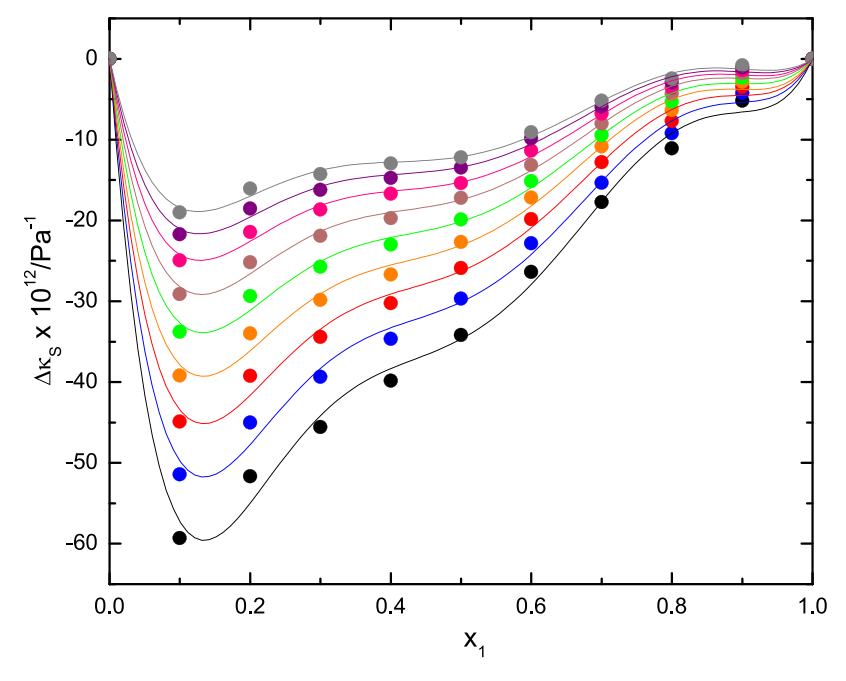


Figure 6. Isentropic compressibility deviation, $\Delta \kappa_S \times 10^{12}/Pa^{-1}$, of ChCl/BA DES—water mixtures as a function of x_1 in the temperature range 303.15 $\leq T/K \leq$ 343.15 (\bullet : 303.15 K; solid blue circle: 308.15 K; solid red circle: 313.15 K; solid orange circle: 318.15 K; solid green circle: 323.15 K; solid brown circle: 328.15 K; solid pink circle: 333.15 K; solid purple circle: 338.15 K; solid gray circle: 343.15 K). The solid lines are the best fit representations of eq 10.

ı

pressure. The validity of eq 16 depends on the behavior of acoustic waves, which does not relax completely under the time constant of these waves.⁶⁹

Figure 5 shows that the κ_S decreases with increasing ChCl/BA DES content in mixtures in the temperature range studied, proposing the slowdown of sound waves and tightening of ChCl/BA DES in aqueous binary mixtures.

Isentropic compressibility deviation $\Delta \kappa_S$ provides information how the molecules are behaving, which is calculated using eq 17.

$$\Delta \kappa_{\rm S} = \kappa_{\rm S} - \sum_{i=1}^{2} x_i \kappa_{\rm s,i} \tag{17}$$

Table 6. Isentropic Compressibility Deviation, $\Delta \kappa_{\rm S} \times 10^{12}/{\rm Pa}^{-1}$, of ChCl/BA DES—Water Mixtures at Different Temperatures T^a

					$\Delta \kappa_{\rm S} \times 10^{12}/{\rm Pa}^{-1}$				
x_1	303.15 K	308.15 K	313.15 K	318.15 K	323.15 K	328.15 K	333.15 K	338.15 K	343.15 K
0.00	0	0	0	0	0	0	0	0	0
0.10	-59.30	-51.44	-44.91	-39.21	-33.78	-29.10	-24.95	-21.72	-18.99
0.20	-51.65	-45.00	-39.25	-33.99	-29.37	-25.18	-21.44	-18.54	-16.06
0.30	-45.55	-39.38	-34.42	-29.84	-25.73	-21.91	-18.67	-16.23	-14.28
0.40	-39.83	-34.64	-30.23	-26.68	-22.98	-19.72	-16.72	-14.73	-12.97
0.50	-34.17	-29.68	-25.92	-22.67	-19.88	-17.21	-15.40	-13.48	-12.22
0.60	-26.39	-22.83	-19.84	-17.20	-15.14	-13.15	-11.36	-9.861	-9.094
0.70	-17.72	-15.33	-12.79	-10.84	-9.447	-8.004	-6.805	-5.944	-5.175
0.80	-11.10	-9.212	-7.721	-6.360	-5.325	-4.304	-3.592	-2.940	-2.437
0.90	-5.186	-4.232	-3.472	-2.825	-2.282	-1.780	-1.402	-1.086	-0.816
1.00	0	0	0	0	0	0	0	0	0

[&]quot;Standard uncertainties, u, in T, x, P, and u are u(T) = 0.01 K, $u(x_1) = 0.01$, u(P) = 10 kPa, and u(u) = 0.5 m·s⁻¹, respectively, and $u(\Delta \kappa_S) = 0.06 \times 10^{-12}$ Pa⁻¹.

Table 7. Intermolecular Free Length, $L_{\rm f} \times 10^{11} / {\rm m}$, of ChCl/BA DES-Water Mixtures as a Function of Mole Fraction x_1^a

					$L_{\rm f} \times 10^{11}/{\rm m}$				
x_1	303.15 K	308.15 K	313.15 K	318.15 K	323.15 K	328.15 K	333.15 K	338.15 K	343.15 K
0.00	4.165	4.174	4.189	4.209	4.233	4.260	4.291	4.326	4.365
0.10	3.785	3.834	3.882	3.930	3.982	4.033	4.086	4.138	4.191
0.20	3.734	3.780	3.827	3.876	3.925	3.976	4.028	4.079	4.131
0.30	3.673	3.721	3.767	3.815	3.864	3.914	3.965	4.014	4.064
0.40	3.610	3.657	3.703	3.748	3.796	3.845	3.895	3.943	3.992
0.50	3.545	3.592	3.638	3.684	3.729	3.777	3.822	3.870	3.916
0.60	3.491	3.537	3.582	3.627	3.670	3.716	3.762	3.808	3.853
0.70	3.441	3.485	3.531	3.575	3.616	3.661	3.705	3.748	3.793
0.80	3.379	3.424	3.467	3.511	3.552	3.596	3.638	3.681	3.725
0.90	3.311	3.355	3.397	3.439	3.480	3.523	3.564	3.606	3.649
1.00	3.237	3.280	3.321	3.362	3.402	3.444	3.484	3.525	3.567

^aStandard uncertainties, u, in T, x, P, and u are u(T) = 0.01 K, $u(x_1) = 0.01$, u(P) = 10 kPa, and u(u) = 0.5 m·s⁻¹, respectively.

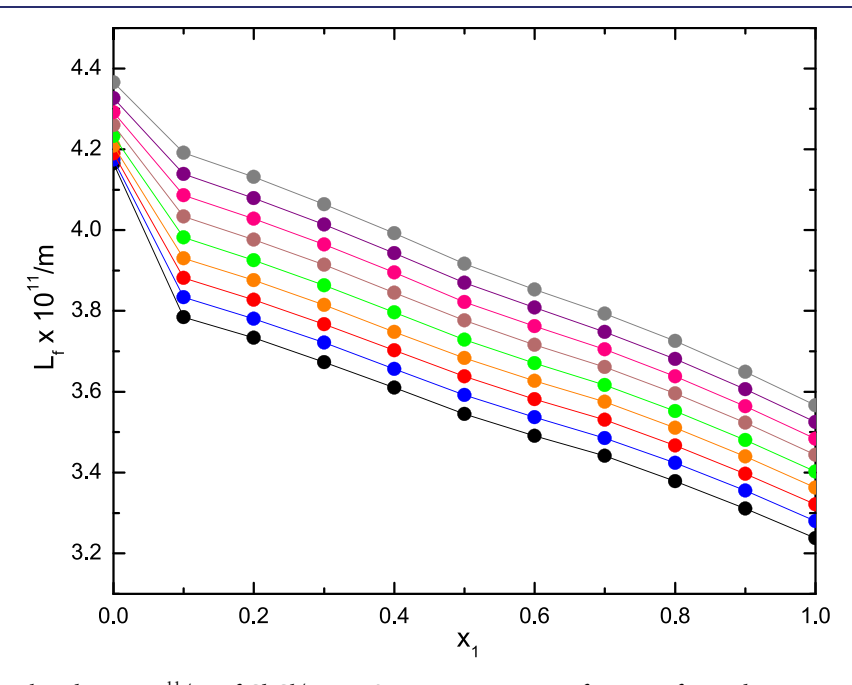


Figure 7. Intermolecular free length, $L_f \times 10^{11}$ /m, of ChCl/BA DES—water mixtures as a function of x_1 in the temperature range 303.15 ≤ $T/K \le$ 343.15 (©: 303.15 K; solid blue circle: 308.15 K; solid red circle: 313.15 K; solid orange circle: 318.15 K; solid green circle: 323.15 K; solid brown circle: 328.15 K; solid pink circle: 333.15 K; solid purple circle: 338.15 K; solid gray circle: 343.15 K). The solid lines connect data points, according to eq 18.

Table 8. Acoustic Impedance, $Z \times 10^{-6}/\text{kg} \cdot \text{m}^{-2} \cdot \text{s}^{-1}$, of ChCl/BA DES-Water Mixtures as a Function of Mole Fraction x_1^a

				Z	$\times 10^{-6}/\text{kg}\cdot\text{m}^{-2}\cdot\text{s}$	-1			
x_1	303.15 K	308.15 K	313.15 K	318.15 K	323.15 K	328.15 K	333.15 K	338.15 K	343.15 K
0.00	1.504	1.512	1.518	1.523	1.525	1.526	1.526	1.524	1.521
0.10	1.666	1.657	1.648	1.638	1.628	1.618	1.608	1.598	1.588
0.20	1.692	1.683	1.674	1.664	1.654	1.644	1.633	1.624	1.613
0.30	1.722	1.712	1.703	1.693	1.683	1.672	1.662	1.652	1.643
0.40	1.755	1.744	1.735	1.726	1.715	1.705	1.694	1.684	1.674
0.50	1.790	1.779	1.769	1.759	1.749	1.739	1.730	1.720	1.710
0.60	1.822	1.811	1.801	1.791	1.782	1.772	1.762	1.752	1.743
0.70	1.852	1.842	1.830	1.820	1.812	1.802	1.792	1.783	1.773
0.80	1.889	1.877	1.867	1.857	1.847	1.837	1.828	1.818	1.809
0.90	1.930	1.918	1.908	1.897	1.888	1.878	1.868	1.859	1.849
1.00	1.977	1.965	1.954	1.943	1.934	1.923	1.914	1.904	1.894

[&]quot;Standard uncertainties, u, in T, x, P, and u are u(T) = 0.01 K, $u(x_1) = 0.01$, u(P) = 10 kPa, and u(u) = 0.5 m·s⁻¹, respectively.

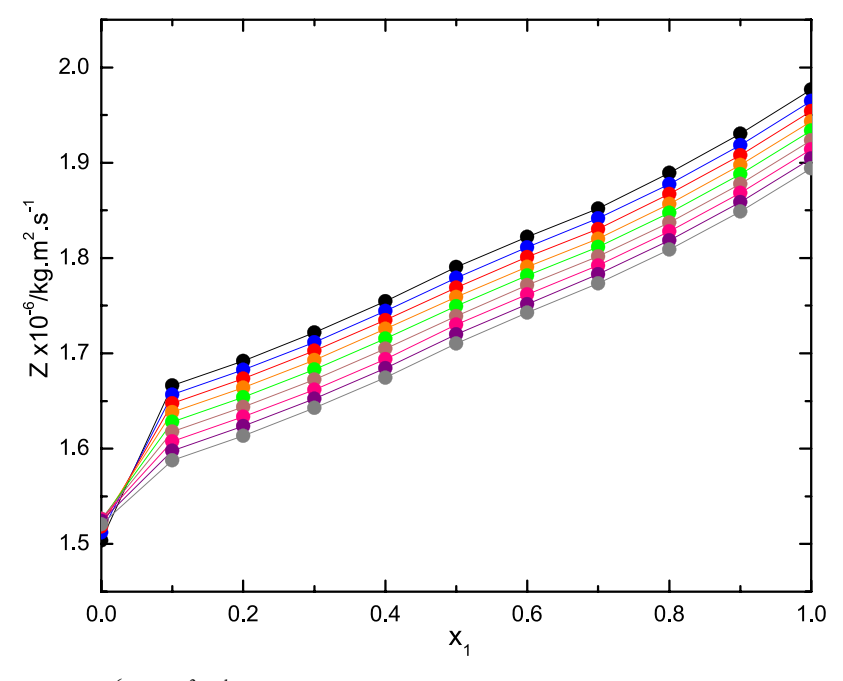


Figure 8. Acoustic impedance, $Z \times 10^{-6}$ /kg·m⁻²·s⁻¹, of ChCl/BA DES—water mixtures as a function of x_1 in the temperature range 303.15 ≤ T/K ≤ 343.15 (\odot : 303.15 K; solid blue circle: 308.15 K; solid red circle: 313.15 K; solid orange circle: 318.15 K; solid green circle: 323.15 K; solid brown circle: 328.15 K; solid pink circle: 333.15 K; solid purple circle: 338.15 K; solid gray circle: 343.15 K). The solid lines connect data points calculated from eq 20.

where x_i and $\kappa_{S,i}$ are mole fractions and isentropic compressibility of component i, respectively.⁷⁰

 $\Delta \kappa_{\rm S}$ vs $\kappa_{\rm 1}$ (Figure 6) explains the packing/interaction among the components of mixtures similar to $V^{\rm E}$, highlighting the identical nature of contributing factors to intermolecular interactions.

The negative values of $\Delta\kappa_{\rm S}$ (Table 6) for the entire range of composition at T=303.15-343.15 K describe stronger interactions between unlike molecules of ChCl/BA DES and water. This indicates that the mixture may be less compressible than the corresponding ideal mixtures due to strong interactions and closer packing between unlike components. The minima in $\Delta\kappa_{\rm S}$ vs x_1 plots for all studied temperatures lie at $x_1\approx 0.15$, which is in the water-rich region. The larger magnitude of $\Delta\kappa_{\rm S}$ values compared to $V^{\rm E}$ shows that sound waves greatly disturbed the system, favoring stronger dipole—dipole interactions and facilitating the interstitial accommodation of molecules of unequal sizes into each other. The

difference in size and shape of component molecules of the binary mixture has a pronounced effect on the sign and magnitude of $\Delta \kappa_{\rm S}$ values. $\Delta \kappa_{\rm S}$ values become less negative with increasing T due to fewer interactions between DES and water at elevated temperatures.

The calculated $\Delta\kappa_S$ is fitted to the Redlich–Kister polynomial equation, eq 10, and the correlated parameters are collected in Table S14 (Supporting Information).

3.2.2. Intermolecular Free Length and Acoustic Impedance. Intermolecular free length $(L_{\rm f})$ is an important acoustical parameter describing the nature and strength of intermolecular and intramolecular interactions existing in the liquid mixture. $L_{\rm f}$ (eq 18) is considered as the distance between the surfaces of the molecules.

$$L_{\rm f} = K \sqrt{\frac{1}{\rho u^2}} \tag{18}$$

Table 9. Dynamic Viscosity, η /mPa·s, of ChCl/BA DES-Water Mixtures as a Function of Temperature T = 303.15 - 343.15 K and Pressure P = 0.1 MPa^a

					$\eta/\text{mPa·s}$				
x_1	303.15 K	308.15 K	313.15 K	318.15 K	323.15 K	328.15 K	333.15 K	338.15 K	343.15 K
0.00	0.797	0.709	0.653	0.596	0.546	0.504	0.466	0.432	0.397
0.10	1.837	1.617	1.439	1.305	1.179	1.073	0.980	0.941	0.882
0.20	3.337	2.663	2.136	1.806	1.562	1.452	1.370	1.274	1.194
0.30	4.228	3.261	2.512	2.037	1.802	1.671	1.565	1.487	1.405
0.40	6.148	4.448	3.241	2.566	2.339	2.174	1.988	1.869	1.763
0.50	9.146	6.526	4.855	3.560	3.262	3.017	2.956	2.838	2.729
0.60	14.27	10.85	8.350	6.517	5.116	4.106	3.883	3.705	3.764
0.70	19.95	16.18	13.20	11.14	9.352	8.090	7.637	7.431	7.399
0.80	25.79	20.89	17.21	14.58	12.28	10.57	9.889	9.450	9.327
0.90	32.05	26.26	21.94	18.77	16.08	14.06	13.30	12.63	12.27
1.00	38.52	31.63	26.35	22.28	18.93	16.36	15.20	14.30	13.65

^aStandard uncertainties, u, in T, x, P, and η are u(T) = 0.01 K, $u(x_1) = 0.01$, u(P) = 10 kPa, and $u_r(\eta) = 0.10$, respectively.

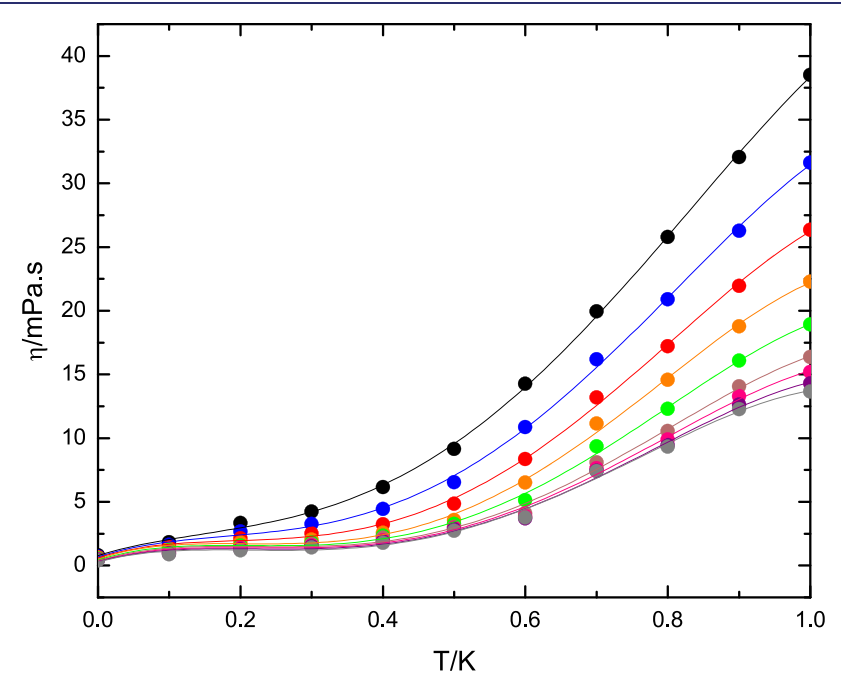


Figure 9. Variation of viscosity η of ChCl/BA DES + water mixtures with the mole fraction of ChCl/BA DES, x_1 , in the temperature range 303.15 ≤ $T/K \le 343.15$ (Φ: 303.15 K; solid blue circle: 308.15 K; solid red circle: 313.15 K; solid orange circle: 318.15 K; solid green circle: 323.15 K; solid brown circle: 328.15 K; solid pink circle: 333.15 K; solid purple circle: 338.15 K; solid gray circle: 343.15 K). The solid lines connecting the data points are the best fit representation of eq 21.

where K is Jacobson's constant, a temperature-dependent parameter.⁷² The calculated values of $L_{\rm f}$ are collected in Table 7, and the plot of $L_{\rm f}$ vs x_1 at T=303.15-343.15 K is shown in Figure 7.

 $L_{\rm f}$ decreases with increasing DES content in aqueous binary mixtures, whereas the influence of T is following the opposite trend. This behavior of $L_{\rm f}$ on x_1 and T is indicative of structural readjustments in mixtures because of the specific interactions between unlike molecules, suggesting the less compressible phase or the closer packing among molecules. The observed behavior is ascribed to the slowing down of speed of sound waves at higher temperatures. The observed behavior is ascribed to the slowing down of speed of sound waves at higher temperatures.

Acoustic impedance Z measures the resistance of ultrasound waves through the medium and is calculated using eq 19.

$$Z = \rho \cdot u \tag{19}$$

The calculated values of Z are collected in Table. 8 and Z vs x_1 are plotted in Figure 8.

Z values increase with increasing T, which indicates the available free space for passage of sound waves. Z increases with increasing DES content in aqueous binary mixtures because sound waves travel faster in less dense medium. This indicates the loosening of the structure as free space is created between the components with increasing concentration.

Variation in acoustic properties ($\Delta \kappa_{\rm S}$, $L_{\rm f}$ and Z) present qualitative description of behavior of the binary mixture (ChCl/BA DES + water) in the intermediate composition range.⁷⁴

3.3. Viscosity. Dynamic viscosity relates the shear force to the degree of fluid resistance and strongly influences the mass and energy transport phenomena of system. 75 η of the DES is influenced by the HBA/HBD mole ratio, molecular mass, temperature, and water content. DESs are relatively more

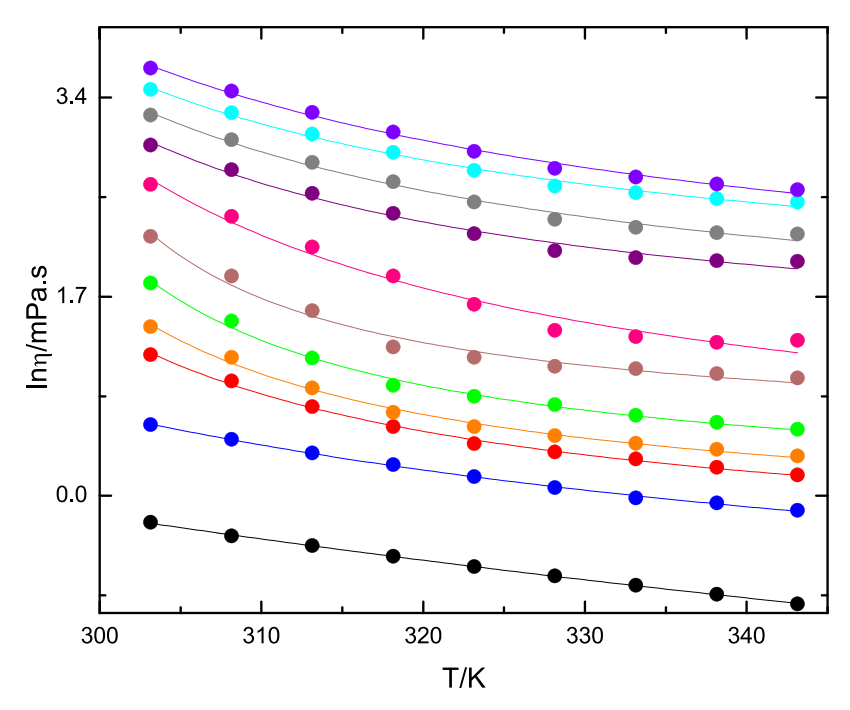


Figure 10. Temperature and composition dependence of dynamic viscosity η for pure ChCl/BA DES, water, and their binary mixtures measured at atmospheric pressure ($x_1 = \Phi$: 0.0; solid blue circle: 0.1; solid red circle: 0.2; solid orange circle: 0.3; solid green circle: 0.4; solid brown circle: 0.5; solid pink circle: 0.6; solid purple circle: 0.7; solid gray circle: 0.8; solid skyblue circle: 0.9; solid violet circle: 1.00). The solid lines are the best fit representations of eq 20.

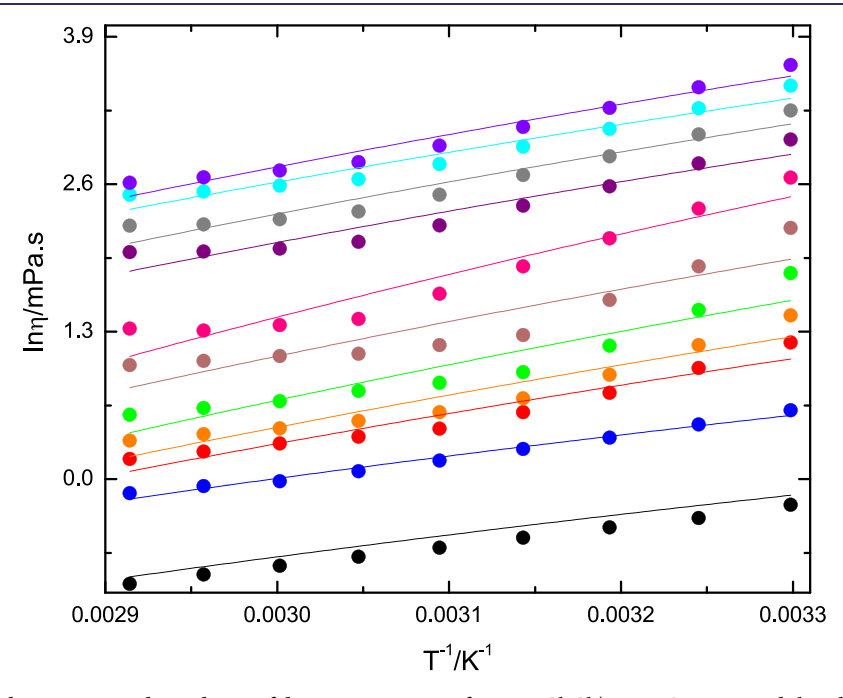


Figure 11. Temperature and composition dependence of dynamic viscosity η for pure ChCl/BA DES, water, and their binary mixtures measured at atmospheric pressure ($x_1 = 0$: 0.0; solid blue circle: 0.1; solid red circle: 0.2; solid orange circle: 0.3; solid green circle: 0.4; solid brown circle: 0.5; solid pink circle: 0.6; solid purple circle: 0.7; solid gray circle: 0.8; solid skyblue circle: 0.9; solid violet circle: 1.00). The solid lines are the best fit representations of eq 23.

viscous than conventional organic solvents, impose restrictions to their practical applications in the chemical process, flow of fluids, mass- and heat-transfer operations, and reaction rate calculations.⁷⁶ It is therefore necessary that their binary mixtures with molecular solvents (e.g., water, alcohols, and DMSO) should be used in design and industrial processes.

In present study, the dynamic viscosity of ChCl/BA DES and its aqueous binary mixtures is measured at temperatures varying in steps of 5 K in the 303.15–343.15 K range, and values are reported in Table 9.

Table 9 shows that η increases with increasing DES content in binary mixtures at T = 303.15-343.15 K and decreases with increasing T for all mole fractions. The concentration

Table 10. Viscosity Deviation $\Delta \eta$ of ChCl/BA DES—Water Binary Mixtures as a Function of ChCl/BA DES Mole Fraction, x_1 , in the Temperature Range 303.15 $\leq T/K \leq 343.15^a$

					$\Delta\eta/\text{mPa·s}$				
x_1	303.15 K	308.15 K	313.15 K	318.15 K	323.15 K	328.15 K	333.15 K	338.15 K	343.15 K
0.00	0	0	0	0	0	0	0	0	0
0.10	-2.731	-2.184	-1.784	-1.460	-1.205	-1.017	-0.959	-0.877	-0.839
0.20	-5.003	-4.230	-3.656	-3.128	-2.660	-2.223	-2.042	-1.931	-1.853
0.30	-7.884	-6.723	-5.851	-5.065	-4.258	-3.589	-3.319	-3.104	-2.967
0.40	-9.736	-8.628	-7.691	-7.105	-6.459	-5.872	-5.520	-5.108	-4.694
0.50	-10.51	-9.642	-8.648	-7.880	-7.174	-6.704	-6.174	-5.526	-4.993
0.60	-9.154	-8.409	-7.723	-7.091	-6.458	-5.910	-5.420	-5.045	-4.582
0.70	-7.250	-6.167	-5.445	-4.638	-4.060	-3.512	-3.140	-2.705	-2.272
0.80	-5.184	-4.549	-4.006	-3.369	-2.967	-2.621	-2.360	-2.072	-1.669
0.90	-2.691	-2.274	-1.840	-1.349	-1.006	-0.715	-0.427	-0.283	-0.050
1.00	0	0	0	0	0	0	0	0	0

"Standard uncertainties, u, in T, x, P, and η are u(T) = 0.01 K, $u(x_1) = 0.01$, u(P) = 10 kPa, $u_r(\eta) = 0.10$, and $u(\Delta \eta) = 0.10$ mPa·s, respectively.

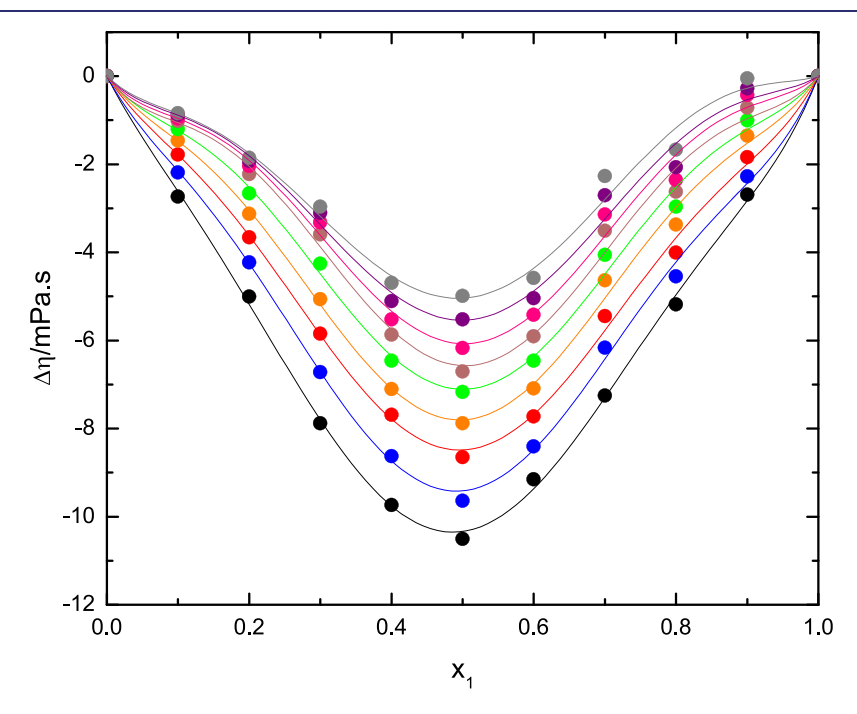


Figure 12. Viscosity deviation $\Delta \eta$ of ChCl/BA DES—water binary mixtures as a function of x_1 in the temperature range 303.15 $\leq T/K \leq$ 343.15 (\bullet : 303.15 K; solid blue circle: 308.15 K; solid red circle: 313.15 K; solid orange circle: 318.15 K; solid green circle: 323.15 K; solid brown circle: 328.15 K; solid pink circle: 333.15 K; solid purple circle: 338.15 K; solid gray circle: 343.15 K). The solid lines connecting data points are the best fit representation of eq 10.

dependence of η at all temperatures is shown in Figure 9. The experimental dynamic viscosity data are fitted well (eq 4), and the correlated parameters are tabulated in Table S15 (Supporting Information).

3.3.1. Temperature Modeling by Vogel–Fulcher–Tammann and Arrhenius Equations. It can be seen in Figure 10 that there is a decrease in logarithmic viscosity with increasing T. The Vogel–Fulcher–Tamman (VFT) equation (eq 20) is used to model the temperature dependence of transport property (Y) of viscous liquids close to their glass-transition temperature.

$$\ln\left(\frac{Y}{Y^0}\right) = \ln\left(\frac{A_Y}{Y^0}\right) + \frac{B_Y}{T - T_{0,Y}} \tag{20}$$

where *Y* is the viscosity η ($Y^0 = \eta^0 = 1 \text{ mPa}^{-1}$) and A_Y , B_Y , and $T_{0,Y}$ are adjustable parameters. The experimental data obtained

at different T values are fitted with the VFT equation (eq 20) by adjusting the VFT parameters. The VFT equation explains that the system kinetics for glass-forming liquids become sluggish on approaching the critical T (or Vogel T), $T_{0,Y}$, which is 10-15 K below the glass-transition temperature, $T_{\rm g}$. The glass-transition temperature ($T_{\rm g}$) decreases with decreasing heating or cooling rate in a supercooled liquid. The VFT equation predicts the divergence of η at finite temperature. η becomes infinite when $T \to T_{0,Y}$. A_Y represents the viscosity as $T \to \infty$, and $E_{\rm a} = B_Y \times R$ (where R is the general gas constant) is the pseudoactivation energy. The calculated values of three fitting parameters are collected in Table S16 (Supporting Information).

The Arrhenius equation (eq 21) is also used to correlate the temperature dependence of η .

Table 11. Optimal Parameters Required in PC-SAFT EoS and the Deviations in Liquid Density Considering the Temperature Range 303.15–343.15 K

Fluid	m	σ (Å)	$\varepsilon/k_{\rm B}$ (K)	κ^{AB}	$\varepsilon^{\mathrm{AB}}/k_{\mathrm{B}}$ (K)	$AAD\rho$ %
DES	5.9028	2.9732	359.57	0.77094	6925.30	0.04
water	0.9700	3.0856	326.60	0.03005	1609.84	0.04
overall	0.04					

$$\ln A = \ln A_{\infty} + \frac{E_{\rm a}}{RT} \tag{21}$$

where A represents η , A_{∞} is an empirical constant, $E_{\rm a}$ is the activation energy associated with the property A, and R and T have their usual meaning. The Arrhenius equation explains the behavior of η as a function of T (Figure 11), which demonstrates the exponential decrease in property. Equation 21 shows limitations for molecules that have small point charges. The fitting of adjustable parameters (eq 21) from experimental data are listed in Table S17 (Supporting Information).

The mathematical interpretation of Arrhenius equation points toward the linear and monotonic increase of transport property with T. The equation is best applicable in the limited temperature range $(T < 2T_g)$.

3.3.2. Viscosity Deviation. Viscosity deviation for viscous fluids is calculated from eq 22.

$$\Delta \eta = \eta - \sum_{i=1}^{2} x_i \eta_i \tag{22}$$

where x_i and η_i are mole fractions and dynamic viscosity of component i, respectively.

The calculated values of $\Delta \eta$ are listed in Table 10, and $\Delta \eta$ vs α_1 at T=303.15-343.15 K is shown in Figure 12.

 $\Delta\eta$ explains the interactions between the DES and cosolvent in terms of (1) loss of dipolar association and difference in the size and shape of component molecules and (2) specific interactions such as charge-transfer complex formation and H-bonding. The former effect corresponds to the negative value of $\Delta\eta$ and the latter explains the positive value of $\Delta\eta$ from the ideal mixing law.

 $\Delta\eta$ values for ChCl/BA DES and its aqueous binary mixtures are negative for the entire composition range for the studied temperature range with minima lying at $x_1 \approx 0.5$. The negative $\Delta\eta$ indicates that weak interaction forces related to the size and shape of molecules are operating in the system, which supports the breaking of self-association of water molecules.

The specific interactions between ChCl/BA DES and water are less dominant in determining the magnitude of the property. The absolute values of $\Delta\eta$ decrease with increasing T, showing the reduction of H-bonding interactions between the DES and cosolvent. Generally, the system showing a positive deviation from ideality for $V^{\rm E}$ also exhibits negative deviations for $\Delta\eta$, which is observed in the present case. The magnitude of $|\Delta\eta|$ (minima at $x_1\approx 0.5$) from ideality is consistent with that of $|V^{\rm E}|$ (maxima at $x_1\approx 0.5$), showing the stability of the aqueous binary mixture in the observed region. The calculated values of $\Delta\eta$ are fitted to the R–K equation (eq 10), and the resulting parameters from regression analysis are reported in Table S18 (Supporting Information).

Intermolecular interactions between DES and water were modeled using the PC-SAFT EoS. Dispersion forces are modeled from the dispersion term present in the equation of state, while dipole—dipole interactions are modeled through the association term, where a 2B scheme is used for DES and a 4C scheme is used for water; i.e., one positive and one negative site are present in DES, while two positive and two negative sites are present in water. The parameters for the DES were obtained using the experimental density data published in this work in the temperature range 303.15–343.15 K and 0.1 MPa pressure, while for water, the vapor pressure of DIPPR data and the density data obtained in this paper were used. Furthermore, the objective functions (OFs) for optimizing the DES and water parameters are described in eqs 23 and 24, respectively:

$$OF\left(m, \sigma, \frac{\varepsilon}{k_{B}}, \frac{\varepsilon^{AB}}{k_{B}}, \kappa^{AB}\right) = \sum_{i=1}^{N} \left(\frac{\rho_{i}^{\text{exp.}} - \rho_{i}^{\text{theo.}}}{\rho_{i}^{\text{exp.}}}\right)^{2}$$

$$OF\left(m, \sigma, \frac{\varepsilon}{k_{B}}, \frac{\varepsilon^{AB}}{k_{B}}, \kappa^{AB}\right)$$

$$= \sum_{i=1}^{N} \left(\frac{P_{i}^{\text{exp.}} - P_{i}^{\text{theo.}}}{P_{i}^{\text{exp.}}}\right)^{2} + \left(\frac{\rho_{i}^{\text{exp.}} - \rho_{i}^{\text{theo.}}}{\rho_{i}^{\text{exp.}}}\right)^{2}$$
(23)

where P is the vapor pressure, N denotes the number of experimental data, and exp. and theo. are related to experimental and theoretical data, respectively. Therefore, the parameters are described in Table 11, from which it is observed that the set of 5 parameters for each fluid correctly fits the density in the liquid phase (overall deviation = 0.04%). Furthermore, the deviation was obtained using eq S4 (Supporting Information).

In this study, the binary interaction parameter (which corrects for dispersion forces between different molecules) was fitted to experimental $V^{\rm E}$ data for each temperature, and the binary interaction parameter exhibits a quadratic temperature dependence in K, given by the following expression: $-7.82109 + 0.045023 \cdot T - 0.000065902 \cdot T^2$, which was obtained by the least-squares method. Therefore, the deviations obtained in ρ and $V^{\rm E}$ using both approaches are illustrated in Table 12.

Table 12. Deviations in ρ and $V^{\rm E}$ Using PC-SAFT and both Approaches

Predictive	e approach	Fitted approach			
$AAD\rho$ %	AADV ^E %	$AAD\rho$ %	AADV ^E %		
0.80	109.09	0.25	34.41		

According to Table 12, PC-SAFT was able to correctly represent the experimental density data quantitatively; the deviations with the predictive and fitted approaches were 0.80 and 0.25%, respectively. On the other hand, with both approaches, the deviations in excess molar volume are high, but the fitted approach manages to reduce the deviation from the predictive approach to 34.41%.

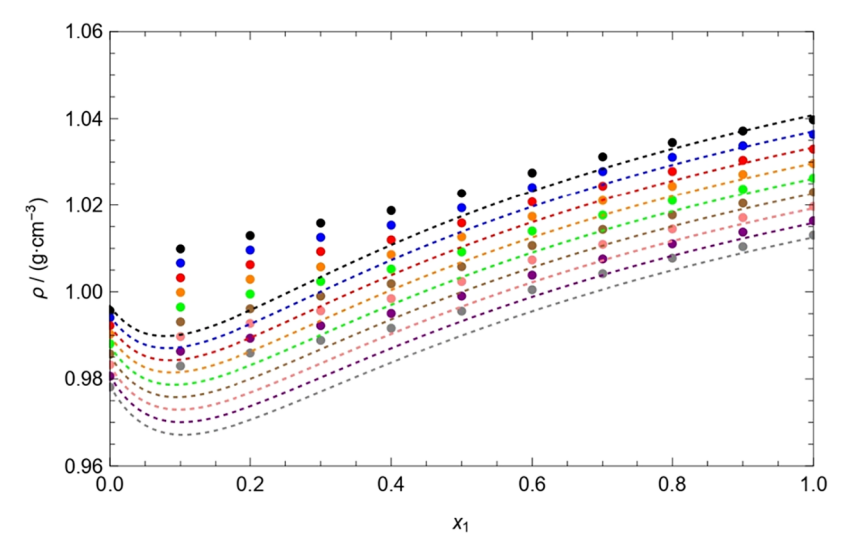


Figure 13. Experimental ρ and calculated values using the predictive approach of PC-SAFT for the DES + water mixture at different temperatures and 0.1 MPa. Circles represent the experimental data (\bullet : 303.15 K; solid blue circle: 308.15 K; solid red circle: 313.15 K; solid orange circle: 318.15 K; solid green circle: 323.15 K; solid brown circle: 328.15 K; solid pink circle: 333.15 K; solid purple circle: 338.15 K; solid gray circle: 343.15 K). Dash lines represent the theoretical results obtained with the PC-SAFT EoS.

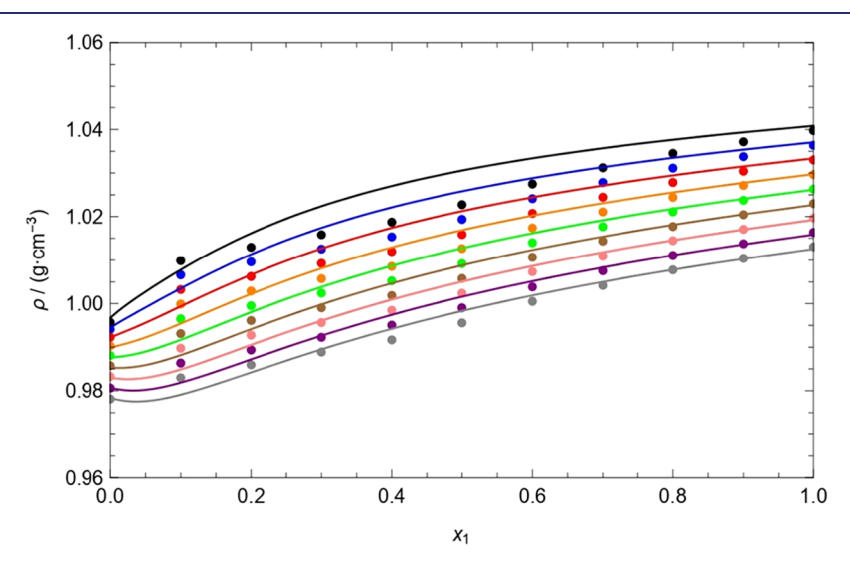


Figure 14. Experimental ρ and calculated values using the fitted approach of PC-SAFT for the DES + water mixture at different temperatures and 0.1 MPa. Circles represent the experimental data (\bullet : 303.15 K; solid blue circle: 308.15 K; solid red circle: 313.15 K; solid orange circle: 318.15 K; solid green circle: 323.15 K; solid brown circle: 328.15 K; solid pink circle: 333.15 K; solid purple circle: 338.15 K; solid gray circle: 343.15 K). Solid lines represent the theoretical results obtained with PC-SAFT EoS.

Figures 13 and 14 show the theoretical results of PC-SAFT for modeling the ρ of the binary mixture using a predictive approach and a fitted approach, respectively. From Figure 13, it is observed that the experimental density data grow monotonically with increasing DES mole fraction. In addition, the predictive approach illustrates curves that present a stationary point at each temperature characterized by a minimum ρ value that decreases with increasing T and that does not agree with the experimental observations. However, although qualitatively PC-SAFT fails to correctly capture the trend in the experimental data, quantitative analysis (Table 12) shows good agreement between the experimental and theoretical density data. On the other hand, Figure 14 shows the theoretical data obtained with the fitted approach, and it is observed that there are temperatures where the curve grows monotonically with the increase in the DES mole fraction and temperatures where stationary points are observed in the

curves. Furthermore, clearly with the fitted approach, the agreement between experimental and theoretical density data is better, as analyzed in Table 12.

Figures 15 and 16 illustrate the experimental data of $V^{\rm E}$ and the theoretical data obtained with the predictive and fitted approaches, respectively. From both figures, it is observed that the $V^{\rm E}$ is positive, which implies that the intermolecular attraction forces are weak and that the repulsive forces predominate; i.e., the mixing volume is greater than the volume of the ideal solution. Furthermore, both figures show that the approaches used are capable of correctly modeling the experimental data of $V^{\rm E}$ from qualitative analysis and that with the fitted approach (see Figure 16), and the experimental data of $V^{\rm E}$ are better represented.

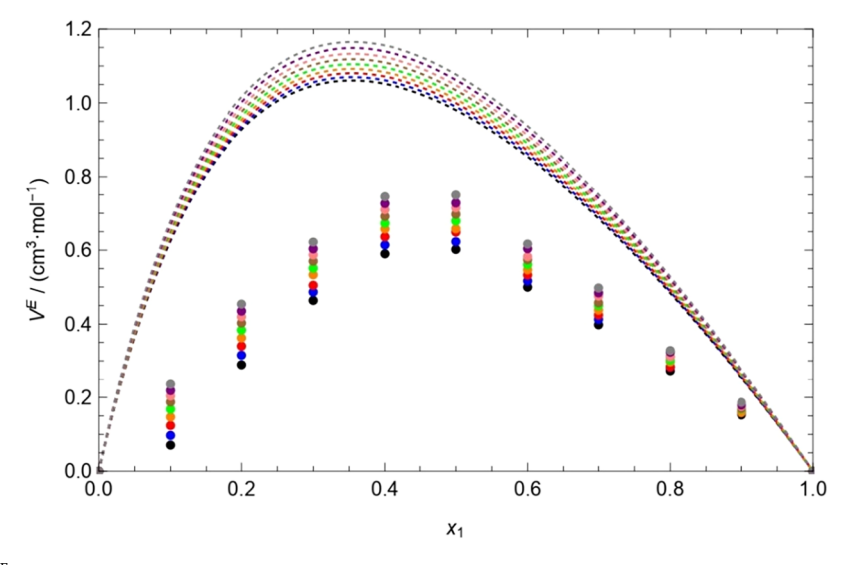


Figure 15. Experimental $V^{\rm E}$ and calculated values using the predictive approach of PC-SAFT for the DES + water mixture at different temperatures and 0.1 MPa. Circles represent the experimental data (\bullet : 303.15 K; solid blue circle: 308.15 K; solid red circle: 313.15 K; solid orange circle: 318.15 K; solid green circle: 323.15 K; solid brown circle: 328.15 K; solid pink circle: 333.15 K; solid purple circle: 338.15 K; solid gray circle: 343.15 K). Dash lines represent the theoretical results obtained with the PC-SAFT EoS.

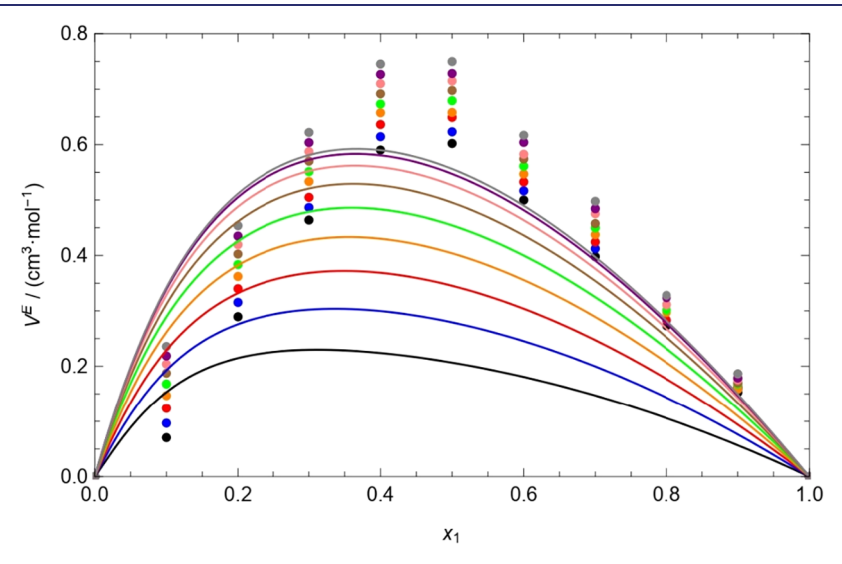


Figure 16. Experimental V^E and calculated values using the fitted approach of PC-SAFT for the DES + water mixture at different temperatures and 0.1 MPa. Circles represent the experimental data (\bullet : 303.15 K; solid blue circle: 308.15 K; solid red circle: 313.15 K; solid orange circle: 318.15 K; solid green circle: 323.15 K; solid brown circle: 328.15 K; solid pink circle: 333.15 K; solid purple circle: 338.15 K; solid gray circle: 343.15 K). Solid lines represent the theoretical results obtained with the PC-SAFT EoS.

4. CONCLUSIONS

In this study, the ChCl/BA DES formed by a combination of choline chloride (ChCl) and butyric acid (BA) is reported and characterized. The density, speed of sound, and dynamic viscosity of ChCl/BA DES and its aqueous binary mixtures are reported over the entire range of composition in the temperature range $303.15 \le T/K \le 343.15$. The experimental density and dynamic viscosity data are fitted well to the fourth-degree polynomial equation in x_1 . To model the density, the second-degree polynomial equation in T satisfactorily explained the temperature dependence of the property. The temperature dependence of dynamic viscosity is compared using VFT and Arrhenius equations. The VFT equation better describes the variation of η with T. Experimental density data are also used to evaluate the lattice energy $(U_{\rm pot})$, molar entropy (S^0) , and intermolecular free length $(L_{\rm f})$ of neat

ChCl/BA DES. Excess properties ($V^{\rm E}$, $\Delta \kappa_{\rm S}$, and $\Delta \eta$) are calculated from measured experimental data and fitted with the Redlich–Kister polynomial equation. The maxima in $V^{\rm E}$ vs x_1 lie at $x_1 \approx 0.5$ at all temperatures support the dominance of nonspecific interactions among the components of DES + water. The minima in $\Delta \eta$ vs x_1 in the temperature range $303.15 \leq T/K \leq 343.15$ is also centered at $x_1 \approx 0.5$, showing the stability of aqueous binary mixtures in the given region. For $\Delta \kappa_{\rm S}$ vs x_1 , the deviation from ideal behavior is in the water-rich region ($x_1 \approx 0.15$), explaining the facilitated interstitial accommodation of component molecules. The calculated AAD for excess properties ($V^{\rm E}$, $\Delta \kappa_{\rm S}$, and $\Delta \eta$) are 0.07 m³· mol⁻¹, 0.08 Pa⁻¹, and 0.2 mPa·s, respectively.

In this study, it is concluded that the equation of state used together with the 2B and 4C association schemes for DES and water, respectively, is able to correctly predict the density of

the binary mixture with a deviation of 0.25%. Furthermore, the quadratic correlation for the binary interaction parameter allowed us to correct the London dispersion forces and reduce the deviation from the predictive approach 109.09% to a value of 34.41%. On the other hand, both PC-SAFT approaches show that the predominant forces are repulsive, which is in agreement with the experimental observations.

ASSOCIATED CONTENT

Supporting Information

The Supporting Information is available free of charge at https://pubs.acs.org/doi/10.1021/acs.jced.5c00423.

FTIR spectra of ChCl/BA DES and its aqueous binary mixtures, 1 H NMR and 13 C NMR spectra of ChCl/BA DES, fit parameters of the R–K equation for excess properties (V^{E} , $\Delta\kappa_{S}$, and $\Delta\eta$), fit parameters of Arrhenius and VFT equations, apparent and partial molar volumes of ChCl/BA DES and water, working principle of DSA 5000, and standard deviation and uncertainty evaluations (PDF)

AUTHOR INFORMATION

Corresponding Authors

Aafia Sheikh — Department of Chemistry, Government College Women University, Sialkot 51310, Pakistan; orcid.org/0000-0001-5861-4425; Email: aafiasheikh300@gmail.com Ariel Hernández — Facultad de Ingeniería y Negocios, Universidad de Las Américas, Concepción 4030000, Chile; orcid.org/0000-0002-6120-9444; Email: ahernandezs@udla.cl

Author

Athar Yaseen Khan — Department of Chemistry, Forman Christian College (A Chartered University), Lahore 54600, Pakistan; orcid.org/0000-0002-8813-5035

Complete contact information is available at: https://pubs.acs.org/10.1021/acs.jced.5c00423

Author Contributions

A.S.: writing—original draft, data acquisition, methodology, analysis, and interpretation of data. A.H.: writing—review and editing, validation, software, and formal analysis. A.Y.K.: writing—review and editing, project administration, validation, supervision, and resources.

Notes

The authors declare no competing financial interest.

ACKNOWLEDGMENTS

The authors are thankful to Dr. Aleeza Farrukh for providing technical feedback.

REFERENCES

- (1) Długosz, O.; Banach, M. Green methods for obtaining deep eutectic solvents (DES). J. Cleaner Prod. 2024, 434, No. 139914.
- (2) Abbott, A. P.; Boothby, D.; Capper, G.; Davies, D. L.; Rasheed, R. K. Deep Eutectic Solvents Formed between Choline Chloride and Carboxylic Acids: Versatile Alternatives to Ionic Liquids. *J. Am. Chem. Soc.* **2004**, *126*, 9142–9147.
- (3) El Achkar, T.; Greige-Gerges, H.; Fourmentin, S. Basics and properties of deep eutectic solvents: a review. *Environ. Chem. Lett.* **2021**, *19*, 3397–3408.
- (4) Smith, E. L.; Abbot, A. P.; Ryder, K. S. Deep Eutectic Solvents (DESs) and Their Applications. *Chem. Rev.* **2014**, *114*, 11060–11082.

- (5) Płotka-Wasylka, J.; Guardia, M. D. L.; Adruch, V.; Vilková, M. Deep eutectic solvents *vs* ionic liquids: Similarities and differences. *Michrochem. J.* **2020**, *159*, No. 105539.
- (6) Moghimi, M.; Roosta, A. Physical properties of aqueous mixtures of (choline chloride + glucose) deep eutectic solvents. *J. Chem. Thermodyn.* **2019**, 129, 159–165.
- (7) Hansen, B. B.; Spittle, S.; Chen, B.; Poe, D.; Zhang, Y.; Klien, J. M.; Horton, A.; Adhikari, L.; Zelovich, T.; Doherty, B. W.; Gurkan, B.; Maggin, E. J.; Ragauskas, A.; Dadmun, M.; Zawodzinski, T. A.; Baker, T. A.; Tuckerman, M. E.; Savinell, R. F.; Sangoro, J. R. Deep Eutectic Solvents: A Review of Fundamentals and Applications. *Chem. Rev.* 2021, 121, 1232–1285.
- (8) Perna, F. M.; Vitale, P.; Capriati, V. Deep eutectic solvents and their applications as green solvents. *Curr. Opin. Green Sustainable Chem.* **2020**, 21, 27–33.
- (9) Söldner, A.; Zach, J.; König, B. Deep eutectic solvents as extraction media for metal salts and oxides exemplarily shown for phosphates from incinerated sewage sludge ash. *Green Chem.* **2019**, 21, 321–328.
- (10) Mbous, Y. P.; Hayyan, M.; Hayyan, A.; Wong, W. F.; Hashim, M. A.; Looi, C. Y. Applications of deep eutectic solvents in biotechnology and bioengineering-Promises and challenges. *Biotechnol. Adv.* **2017**, *35*, 105–134.
- (11) Zhu, A.; Bian, X.; Han, W.; Cao, D.; Wen, Y.; Zhu, K.; Wang, S. The application of deep eutectic solvents in lithium-ion battery recycling: A comprehensive review. *Resour., Conserv. Recycl.* **2023**, *188*, No. 106690.
- (12) Fouji, M.; Khalili, M. R.; Torghabeh, M. A.; Darband, G. B. Deep eutectic electrodeposition for energy storage and conversion systems. A comprehensive review. *Int. J. Hydrogen Energy* **2024**, *69*, 1511–1538.
- (13) Alqahtani, A. S. Indisputable roles of different ionic liquids, deep eutectic solvents and nanomaterials in green chemistry for sustainable organic synthesis. *J. Mol. Liq.* **2024**, 399, No. 124469.
- (14) Yuan, Z.; Liu, H.; Yong, W. F.; She, Q.; Esteban, J. Status and advances of deep eutectic solvents for metal separation and recovery. *Green Chem.* **2022**, *24*, 1895–1929.
- (15) Zaib, Q.; Eckelman, M. J.; Yang, Y.; Kyung, D. Are deep eutectic solvents really green?: A life-cycle perspective. *Green. Chem.* **2022**, 24, 7924–7930.
- (16) Sheikh, A.; Saleem, I.; Ahmed, S.; Abbas, M.; Khan, A. Y. Investigation of physicochemical properties of NADES based on choline chloride and ascorbic acid and its binary solutions with DMSO from (298.15 to 353.15) K. J. Mol. Liq. 2022, 364, No. 120038
- (17) de Morais, P.; Goncalves, F.; Coutonho, J. A. P.; Ventura, S. P. M. Ecotoxicity of Cholinium-Based Deep Eutectic Solvents. *ACS Sustainable Chem. Eng.* **2015**, *3*, 3398–3404.
- (18) Naseem, Z.; Shehzad, R. A.; Jabeen, S.; Tahir, S.; Mushtaq, S. F.; Zahid, M.; Iqbal, J. Quantum chemical investigation of choline chloride-based deep eutectic solvents. *Chem. Phys.* **2023**, *571*, No. 111936.
- (19) Uzochukwu, M. I.; Oyegoke, T.; Momoh, R. O.; Isa, M. T.; Shuwa, S. M.; Jibril, B. Y. Computational insights into deep eutectic solvent design: Modeling interactions and thermodynamic feasibility using choline chloride & glycerol. *Chem. Eng. J. Adv.* **2023**, *16*, No. 100564.
- (20) Ninayan, R.; Levshakova, A. S.; Khairullina, E. M.; Vezo, O. S.; Tumkin, I. I.; A Ostendorf, A.; Logunov, L. S.; Manshina, A. A.; Shishove, A. Y. Water-induced changes in choline chloride-carboxylic acid deep eutectic solvents properties. *Colloids Surf., A* **2023**, *679*, No. 132543.
- (21) Boethling, R. S.; Sommer, E.; Difiore, D. Designing small molecules for biodegradability. *Chem. Rev.* **2007**, *107*, 2207–2227.
- (22) Kelbert, M.; Machado, T. O.; Arujo, P. H. H.; Sayer, C.; de Oliveira, D.; Maziero, P.; Simons, K. E.; Carciofi, B. A. M. Perspectives on biotechnological production of butyric acid from lignocellulosic biomass. *Renew. Sustainable Energy Rev.* **2024**, 202, No. 114717.

- (23) Abdel-Latif, H. M. R.; Abdel-Tawab, M.; Dawood, M. A. O.; Menanteau-Ledouble, S.; El-Matbouli, M. Benefits of Dietary Butyric Acid, Sodium Butyrate, and Their Protected Forms in Aquafeeds: A Review. *Rev. Fish. Sci. Aquacult.* **2020**, *28*, 421–448.
- (24) Barani Pour, S.; Sardroodi, J. J.; Ebrahimzadeh, A. R.; Pazuki, G.; Rezvan, V. H. A comparative study of deep eutectic solvents based on fatty acids and the effect of water on their intermolecular interactions. *Sci. Rep.* **2024**, *14*, No. 1763.
- (25) Shishov, A.; Pochivalov, A.; Nugbienyo, L.; Andruch, V.; Bulatov, A. Deep eutectic solvents are not only effective extractants. *TrAC, Trends Anal. Chem.* **2020**, *129*, No. 115956.
- (26) Aissaoui, T.; AlNashef, I. M.; Qureshi, U. A.; Benguerba, Y. Potential applications of deep eutectic solvents in natural gas sweetening for CO₂ capture. *Rev. Chem. Eng.* **2017**, *33*, 523–550.
- (27) Homan, T.; Shahbaz, K.; Farid, M. M. Improving the production of propyl and butyl ester-based biodiesel by purification using deep eutectic solvents. *Sep. Purif. Technol.* **2017**, *174*, 570–576.
- (28) Kuddushi, M.; Nangala, G. S.; Rajput, S.; Ijardar, S. P.; Malek, N. I. Understanding the peculiar effect of water on the physicochemical properties of choline chloride based deep eutectic solvents theoretically and experimentally. *J. Mol. Liq.* **2019**, 278, 607–615.
- (29) Wang, Y.; Ma, C.; Liu, C.; Lu, X.; Feng, X.; Ji, X. Thermodynamic Study of Choline Chloride-Based Deep Eutectic Solvents with Water and Methanol. *J. Chem. Eng. Data* **2020**, *65*, 2446–2457.
- (30) Zarei, A.; Haghbaksh, R.; Raeissi, S. Overview and thermodynamic modelling of deep eutectic solvents as co-solvents to enhance drug solubilities in water. *Eur. J. Pharm. Biopharm.* **2023**, 193, 1–15.
- (31) Mohsen-Nia, M.; Amiri, H.; Jazi, B. Dielectric constants ofwater, methanol, ethanol, butanol and acetone: Measurement and and acetone study. *J. Solution Chem.* **2010**, *39*, 701–708.
- (32) Zuo, Y.; Chen, X.; Wei, N.; Tong, J. Effect of water or ethanol on the excess properties of deep eutectic solvents (tetrabutylammonium bromide + formic acid/propionic acid). *J. Mol. Liq.* **2023**, 383, No. 122034.
- (33) Gross, J.; Sadowski, G. Perturbed chain SAFT: An equation of state based on a perturbation theory for chain molecules. *Ind. Eng. Chem. Res.* **2001**, *40*, 1244–1260.
- (34) Gross, J.; Sadowski, J. G. Application of the perturbed-chain SAFT equation of state to associating systems. *Ind. Eng. Chem. Res.* **2002**, *41*, 5510–5515.
- (35) Sheikh, A.; Hernández, A.; Khan, A. Y.; Ahmed, S. Physicochemical properties of deep eutectic solvent choline chloride: Propionic acid (ChCl/PA DES) and its binary solutions with 1-butanol as cosolvent. *J. Mol. Liq.* **2025**, 425, No. 127217.
- (36) Zhang, J.; Yin, J.; Zhang, Y.; Zhu, T.; Ran, H.; Jiang, W.; Li, H.; Li, H.; Zhang, M. Insights into the formation mechanism of aliphatic acid-choline chloride deep eutectic solvents by theoretical and experimental research. *J. Mol. Liq.* **2022**, 367, No. 120342.
- (37) Vieira, V.; Prieto, M. A.; Barros, L.; Coutinho, J. A. P.; Ferreira, I. C. F. R.; Ferreira, O. Enhanced extraction of phenolic compounds using choline chloride based deep eutectic solvents from *Juglans regia* L. *Ind. Crops Prod.* **2018**, *115*, 261–271.
- (38) Torbati, M.; Farajzadeh, M. A.; Mogaddam, M. R. A.; Torbati, M. Deep eutectic solvent based homogeneous liquid—liquid extraction coupled with in-syringe dispersive liquid liquid micro-extraction performed in narrow tube; application in extraction and preconcentration of some herbicides from tea. *J. Sep. Sci.* **2019**, *42*, 1768—1776.
- (39) Ghaedi, H.; Ayoub, M.; Sufian, S.; Sharrif, A. M.; Murshid, G.; Hailegiorgis, S. M.; Khan, S. N. Density, Excess and Limiting Properties of (Water and Deep Eutectic Solvent) Systems at Temperatures from 293.15 to 343.15 K. J. Mol. Liq. 2017, 48, 378–390.
- (40) Zarghampour, A.; Jafari, P.; Rahimpour, E.; Jouyban, A. Thermodynamic investigation on the aqueous mixtures of choline

- chloride/propylene glycol deep eutectic solvent at T = (293.15 to 313.15) K. BMC Chem. **2024**, 18, No. 51.
- (41) Yadav, A.; Kar, J. R.; Verma, M.; Naqvi, S.; Pandey, S. Densities of aqueous mixtures of (choline chloride + ethylene glycol) and (choline chloride + malonic acid) deep eutectic solvents in temperature range 283.15–363.15 K. *Thermochim. Acta* 2015, 600, 95–101.
- (42) Agieienko, V.; Buchner, R. Densities, Viscosities, and Electrical Conductivities of Pure Anhydrous Reline and Its Mixtures with Water in the Temperature Range (293.15 to 338.15) K. J. Chem. Eng. Data 2019, 64, 4763–4774.
- (43) Shekaari, H.; Zafarani-Moattar, M. T.; Mohammadi, B. Thermophysical properties of choline chloride/urea deep eutectic solvent in aqueous solution at infinite dilution at T=293.15-323.15 K. J. Therm. Anal. Calorim. **2020**, 139, 3603–3612.
- (44) Mero, A.; Koutsoumpos, S.; Giannios, P.; Stavrakas, I.; Moutzouris, K.; Mezzetta, A.; Guazzelli, L. Comparison of physicochemical and thermal properties of choline chloride and betaine-based deep eutectic solvents: The influence of hydrogen bond acceptor and hydrogen bond donor nature and their molar ratios. *J. Mol. Liq.* 2023, 377, No. 121563.
- (45) Kermanpour, F. Thermodynamic study of binary mixtures of propilophenone + 2-propanol, 2-butanol, 2-pentanol, or 2-hexanol at temperatures of 293.15 to 323.15 K: Modeling by Prigogine-Flory-Patterson theory. *J. Mol. Liq.* **2023**, *376*, No. 121448.
- (46) Glasser, L. Lattice and phase transition thermodynamics of ionic liquids. *Thermochim. Acta* **2004**, 421 (1–2), 87–93.
- (47) Lide, D. R. CRC Handbook of Chemistry and Physics, 85th ed.; CRC Press, 2004.
- (48) Shi, Y.; Liu, S.; Wang, S.; Yu, Y.; Chen, X.; Zhu, X. Thermodynamic properties of DBN-based ionic liquids and their binary mixtures with primary alcohols. *J. Mol. Liq.* **2023**, *371* (2023), No. 121060.
- (49) Singh, K.; Shibu, R. P.; Mehra, S.; Kumar, A. Insights into the physicochemical properties of newly synthesized benzyl triethylammonium chloride-based deep eutectic solvents. *J. Mol. Liq.* **2023**, 386, No. 122589.
- (50) Gao, J.; Yang, X.; Xing, Z.; Song, X.; Liu, Y.; Wang, Z.; Deng, G.; Zhao, X. Physicochemical and thermodynamic properties of binary amine-based deep eutectic solvents for carbon capture. *J. Mol. Lia.* 2024, 399, No. 124346.
- (51) Priya, J. J.; Duraivathi, C.; Poongodi, J.; Amudhavalli, K. Excess thermodynamic properties of binary liquid mixture at different temperature. *Mater. Today* **2012**, *49*, 1810–1814.
- (52) Trenzado, J. L.; Rodriguez, Y.; Gutierrez, A.; Cincotti, A.; Aparicio, S. Experimental and molecular modeling study on the binary mixtures of [EMIM][BF4] and [EMIM][TFSI] ionic liquids. *J. Mol. Liq.* 2021, 334, No. 116049.
- (53) Nain, A. K.; Nidhi; Chaudhary, N. Excess acoustic and volumetric properties of polyethylene glycol 200 + methyl/ethyl methacrylate binary mixtures at different temperatures: An experimental and theoretical study. *J. Chem. Thermodyn.* **2025**, 200, No. 107358.
- (54) Haghbakhsh, R.; Raeissi, S. Excess volumes of mixtures consisting of deep eutectic solvents by the Prigogine—Flory—Patterson theory. *J. Mol. Liq.* **2018**, 272, 731–737.
- (55) Vural, U. S.; Muradoglu, V.; Vural, S. Excess molar volume and refractive index of binary mixtures of glycerol + methanol and glycerol + water at 298.15 and 303.15 K. *Bull. Chem. Soc. Ethiop.* **2011**, 25, 111–118.
- (56) Gahlyan, S.; Rani, M.; Maken, S. Excess molar volume of binary mixtures containing an oxygenate. *J. Mol. Liq.* **2014**, *199*, 42–50.
- (57) Tao, Y.; Zou, W.; Jia, J.; Cremer, D. Different Ways of Hydrogen Bonding in Water Why Does Warm Water Freeze Faster than Cold Water? *J. Chem. Theory Comput.* **2017**, *13*, 55–76.
- (58) Patyar, P.; Ali, A.; Malek, N. I. Experimental and theoretical excess molar properties of aqueous choline chloride based deep eutectic solvents. *J. Mol. Lig.* **2021**, *324*, No. 114340.

- (59) Sharma, R.; Athira, K. K.; Gardas, R. L.; Malek, N.; Ijardar, S. P. Physicochemical and acoustic characterization of binary mixtures of tetraalkylammonium bromide: PEG based DES and water. *J. Mol. Liq.* **2022**, *367*, No. 120386.
- (60) Jangir, A. K.; Nain, A. K.; Kuperkar, K. Insight into structural properties and molecular interactions of maline (choline chloride + malonic acid) and 1, 4-butanediol based pseudo-binary mixture: A thermophysical, spectral, and simulation portrayal. *J. Mol. Liq.* **2021**, 334, No. 116050.
- (61) Jha, S. M.; Athira, K. K.; Gardas, R.; Malek, N.; Ijardar, S. P. Unveiling the Molecular Interactions in an Aqueous Binary System of Guanidine Hydrochloride-Based Deep Eutectic Solvents: Physicochemical Properties and Spectroscopic Approach. *J. Chem. Eng. Data* **2025**, 70, 2631–2644.
- (62) Verma, S.; Kashyap, P.; Rani, M.; Song, H.; Maken, S. Volumetric, acoustic, and optical properties of binary mixtures of diethyl ether with alkanol at T = 293.15 to 303.15 K. *J. Mol. Liq.* **2024**, 394, No. 123796.
- (63) Redlich, O.; Kister, A. T. Thermodynamics of non-electrolyte solutions, x-y-t relation in binary system. *Ind. Eng. Chem.* **1948**, *40*, 341–345
- (64) Kim, K.-S.; Park, B. H. Volumetric Properties of Solutions of Choline Chloride + glycerol Deep Eutectic Solvent with Water Methanol. Ethanol. or Iso-Propanol. *J. Mol. Liq.* **2018**, 254, 272–279.
- (65) Carissimi, G.; Montalban, M. G.; Banos, F. G. D.; Villora, G. Density, Refractive Index and Volumetric Properties of Water–Ionic Liquid Binary Systems with Imidazolium-Based Cations and Tetrafluoroborate, Triflate and Octylsulfate Anions at T = 293 to 343 K and p = 0.1 MPa. *J. Chem. Eng. Data* **2019**, *64*, 979–994.
- (66) Anouti, M.; Vigeant, A.; Jacquemin, J.; Brigouleix, C.; Lemordant, D. Volumetric properties, viscosity and refractive index of the protic ionic liquid, pyrrolidinium octanoate, in molecular solvents. *J. Chem. Thermodyn.* **2010**, *42*, 834–845.
- (67) Shekaari, H.; Zafarani-Moattar, M. T.; Mokhtarpour, M.; Faraji, S. Effect of some choline based deep eutectic solvents on volumetric and ultrasonic properties of gabapentin drug in water at T = (288.15 to 318.15) K. *J. Mol. Liq.* **2022**, *346*, No. 117073.
- (68) Abdel Jabbar, N. M.; Mjalli, F. S. Ultrasonic study of binary aqueous mixtures of three common eutectic solvents. *Phys. Chem. Liq.* **2019**, *57*, 1–18.
- (69) Davis, M. I.; Douheret, G.; Reis, J. C. R.; Blandamer, M. J. Apparent and partial ideal molar isentropic compressibilities of binary liquid mixtures. *Phys. Chem. Chem. Phys.* **2001**, *3*, 4555–4559.
- (70) Prak, D. J. L.; Prak, L. n-Pentadecane and n-Alkylcyclohexane Mixtures: Viscosity Deviations and Excess Molar Volumes, Speeds of Sound, and Isentropic Compressibilities at 0.1 MPa. *J. Chem. Eng. Data* **2023**, *68*, 2198–2211.
- (71) Nowosielski, B.; Jamrógiewicz, M.; Łuczak, J.; Warmińska, D. Novel Binary Mixtures of Alkanolamine Based Deep Eutectic Solvents with Water—Thermodynamic Calculation and Correlation of Crucial Physicochemical Properties. *Molecules* **2022**, *27*, No. 788.
- (72) Jacobson, B. Ultrasonic Velocity in Liquids and Liquid Mixtures. J. Chem. Phys. 1952, 20, 927–928.
- (73) Pathania, V.; Sharma, S.; Vermani, B. K.; Gill, D. S. A study of some excess thermodynamic properties in binary mixtures of non-aqueous solvents at variable temperatures. *Phys. Chem. Res.* **2022**, *10*, 439–453.
- (74) Jangir, A. K.; Mandviwala, H.; Patel, P.; Sharma, S.; Kuperkar, K. Acumen into the effect of alcohols on choline chloride: L-lactic acid-based natural deep eutectic solvent (NADES): A spectral investigation unified with theoretical and thermophysical characterization. *J. Mol. Liq.* **2020**, *317*, No. 113923.
- (75) Pinho, M. R.; Lima, A. S.; Oliveira, G. D. A. R.; Liao, L. M.; Franceschi, E.; Silva, R. D.; Cardozo-Filho, L. Choline Chloride- and Organic Acids-Based Deep Eutectic Solvents: Exploring Chemical and Thermophysical Properties. *J. Chem. Eng. Data* **2024**, *69*, 3403–3414. (76) Haghbakhsh, R.; Parvaneh, K.; Raeissi, S.; Shariati, A. A general viscosity model for deep eutectic solvents: The free volume theory

- coupled with association equations of state. Fluid Phase Equilib. 2018, 470, 193–202.
- (77) Abed, K. M.; Hayyan, A.; Hizzadin, H. F.; Basirun, W. J.; Hashim, M. A. Lactic acid-based deep eutectic solvents and activated carbon for soap removal from crude biodiesel. *Biomass Convers. Biorefnery* **2024**, *14*, 17805–17818.
- (78) Gao, Q.; Jian, Z. Fragility and Vogel-Fulcher-Tammann parameters near glass transition temperature. *Mater. Chem. Phys.* **2020**, 252, No. 123252.
- (79) Zuo, Z.; Cao, B.; Wang, Y.; Ma, C.; Lu, X.; Ji, Z. Thermodynamic study of choline chloride-based deep eutectic solvents with dimethyl sulfoxide and isopropanol. *J. Mol. Liq.* **2024**, 394, No. 123731.
- (80) Mahajan, A. R.; Mirgane, S. R. Excess molar volumes and viscosities for the binary mixtures of n-octane, n-decane, n-dodecane, and n-tetradecane with octan-2-ol at 298.15 K. *J. Thermodyn.* **2013**, 2013, 1–11.
- (81) Daubert, T. E.; Danner, R. P. Physical and Thermodynamic Properties of Pure Chemicals: Data Compilation; Taylor & Francis: Bristol, PA, 2004.

